UNIVERSITÀ POLITECNICA DELLE MARCHE
Department of Agricultural, Food and Environmental Sciences (D3A)
PhD Course in Agricultural, Food and Environmental Sciences (XXXV cycle)

Molecular insights into plant proteins involved in NAD^+ biosynthesis and signalling

Advisor:
Prof.ssa Nadia Raffaelli

Ph.D. dissertation of:
Carlo Fortunato

Academic years 2019/2020 - 2021/2022

CONTENTS

Chapter I
INTRODUCTION 4
Vitamin B3 5
NAD^+ metabolism in plants 6
NAD^+ signalling in plants 8
References 10

Chapter II
OUTLINE OF THE THESIS 14

Chapter III
MOLECULAR AND STRUCTURAL CHARACTERIZATION OF *A.thaliana* NaMN/NMN ADENYLYLTRANSFERASE 16
INTRODUCTION 17
NaMN/NMN adenylyltransferases overview 17
Plant NaMN/NMN adenylyltransferase 22
EXPERIMENTAL PROCEDURES 22
Cloning, Expression and Purification 22
Enzymatic activity determination 24
Spectrophotometric assay 24
HPLC-based assay 24
Molecular weight determination 25
Catalytic characterization 25
Effect of NAD^+ metabolites 25
Kinetic characterization 25
Crystallization, Data collection and Structure Determination 26
Site-directed mutagenesis 29
RESULTS AND DISCUSSION 29
Production and molecular characterization of the recombinant enzyme 29
Catalytic characterization 31
Structural characterization 34
Structure of the apo-enzyme 34
Structure of the enzyme in complex with NaMN and NMN 37
Structure of the enzyme in complex with NaAD and NAD^+ 39
Dual substrate specificity 42
References 45

Chapter IV
PRODUCTION OF EXTRACELLULAR DOMAIN OF LECRK1.8 RECEPTOR 52
INTRODUCTION 53
EXPERIMENTAL PROCEDURES 54
Molecular cloning of eLecRK 1.8 54
Insect cells transfection and virus amplification 55
Plaque assay 55
Expression of eLecRK 1.8 56
Western blot analysis 56
RESULTS .....
Production of the extracellular domain of LecRK 1.8 57
References 60

Chapter V
CONCLUSIONS 62

CHAPTER I

INTRODUCTION

1.1. Vitamin B3

B3 vitamin, or niacin, is an essential compound for human nutrition and its deficiency has been associated with pellagra, Reynaud's disease, osteoarthritis and many mental disorders, such as amnesia, apathy and depression. At the same time, a correct niacin uptake is strictly linked with the prevention of metabolic, cardiovascular and neurodegenerative disorders (Helman and Braidy 2022; Schmeisser and Parker 2018; Lee et al. 2016). Humans primarily obtain vitamin B3 from plant sources, especially grains, vegetables, legumes and plants derived oils. However, the B3 vitamin content strongly depends on species, cultivars and storage organs. For this reasons, the deep comprehension of the B3 vitamin metabolism in plants has acquired great importance during last century (Lebiedzińska and Szefer 2006).

Niacin is a generic term which refers to nicotinic acid, nicotinamide and nicotinamide riboside. These molecules are all precursors of Nicotinamide Adenine Dinucleotide (NAD^+), which is the biologically active form of the vitamin (Figure 1).

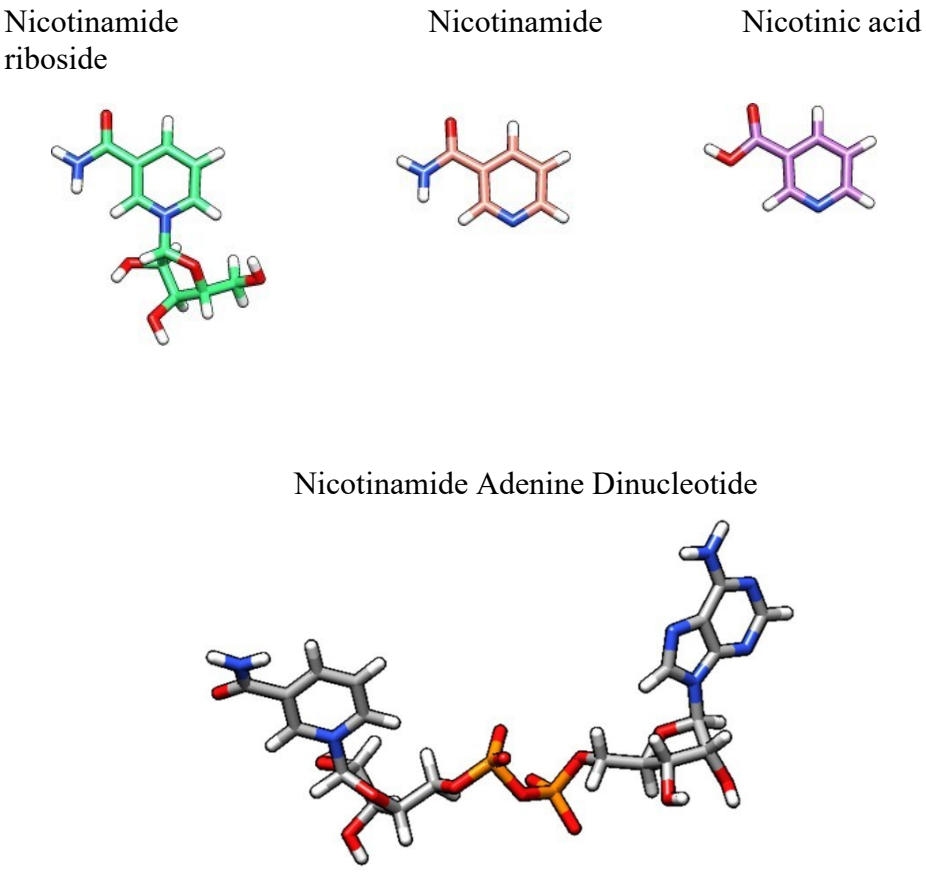

Figure 1. Structures of the three forms of vitamin B3 and NAD^+.

1.2. NAD^+ metabolism in plants

NAD^+ is a ubiquitous molecule used by all living cells as the redox coenzyme of dehydrogenases. As an example, NAD^+ is reduced to NADH in catabolic reactions of energetic metabolism and NADH is re-oxidized to NAD^+ in mitochondrial electron transfer chain, thus driving ATP generation (Katoh and Hashimoto 2004).

The importance of NAD^+/NADH, as well as their phosphorylated counterparts $NADP^+$/NADPH ratios in tuning cellular redox state and therefore affecting photosynthesis, energy production and consumption, is known since the beginning of last century.
Besides being used as a coenzyme by dehydrogenases, NAD^+ can behave as a substrate for different enzymes of relevance in many cellular processes. Among them are:

- *NAD^+ Kinase*, which catalyses NAD^+ phosphorylation to $NADP^+$
- *NAD^+ pyrophosphatase* of the Nudix hydrolase family, which cleaves NAD^+ to AMP and NMN and is involved in stress response and in processes like seed germination, plant growth and development;
- *ADP-Ribosyl-cyclase*, which forms cyclic ADP ribose (ADPR), an important second messenger that mobilizes intracellular calcium (Morgan and Galione 2008) and influences oxidative balance interacting in abscisic acid (ABA) signal transduction (Wu et al. 1997);
- *Poly(ADP-ribose)polymerases (PARPs)* and *Poly(ADP-ribose)glycohydrolases (PARGs)*, which together with *Sirtuins* are enzymes involved in DNA repair, apoptosis, chromatin remodelling, control of gene transcription by covalent modification (either ADP-ribosylation or deacetylation) of specific transcription factors or histones.

In general, NAD^+ biosynthesis can occur *de novo* through two different routes: the aspartate pathway, that starts from L-Aspartic acid and is a typical prokaryotic pathway, and the kynurenine pathway, that starts from L-Tryptophan, and is mostly present in eukaryotes. In plants, it has been demonstrated that aspartate pathway is always present and occurs in plastids. Both in dicotyledons and monocotyledons' chloroplasts, the enzymes L-Asp oxidase and quinolinate synthase convert aspartic acid to quinolinic acid (Qa), the substrate of quinolinic acid phosphoribosyl transferase (QaPRT)(Katoh et al. 2006) (Figure 2). This enzyme forms nicotinate mononucleotide (NaMN), that crosses the chloroplast membrane. NaMN can also be formed in the cytosol by the enzyme nicotinate phosphoribosyl transferase (NaPRT) starting from nicotinic acid (Na) (Hunt, Lerner, and Ziegler 2004; Yamada et al. 2003). The enzyme NaMN adenylyltransferase (NaMNAT) utilizes NaMN deriving from both plastids and NaPRT activity and produces nicotinate adenine dinucleotide (NaAD)

(Hashida et al. 2007). NaAD is finally amidated to NAD^+ by the enzyme NAD^+ synthase (NADS). A NMN adenylyltransferase (NMNAT) activity, able to convert NMN into NAD^+, was observed in artichoke mitochondria (Di Martino and Pallotta 2011) (Figure 2). $NADP^+$ is produced from NAD^+ by NAD^+ kinase (NADK) (Waller et al. 2010) (Figure 2). Five genes coding for the enzymes of kynurenine pathway have been found in monocotyledons' genome, thus leading to the hypothesis that this clade may also synthetize NAD^+ from L-Tryptophan (Katoh and Hashimoto 2004). The reactions from Qa to NAD^+ are common to both the kynurenine pathway and the aspartate pathway and are conserved in all organisms.

Besides the *de novo* pathway, NAD^+ can be formed through several different routes collectively known as the salvage pathways. Most of the enzymes that use NAD^+ as substrate release nicotinamide (Nam) and the most representative salvage pathway recycles back Nam to NAD^+. In plants, Nam is first deamidated to Na by the enzyme nicotinamidase, for which three isoforms have been identified in *Arabidopsis* (Wang and Pichersky 2007; Hunt, Holdsworth, and Gray 2007; Schippers et al. 2008). Na then enters the *de novo* pathway after its conversion to NaMN by the enzyme NaPRT (Figure 2). Nicotinamide riboside (NR) enters the NAD^+ biosynthetic pathway through its conversion into NMN which is catalysed by the enzyme nicotinamide riboside kinase (NRK) (Katahira and Ashihara 2009; Matsui and Ashihara 2008). Nicotinamide, nicotinamide riboside and nicotinic acid present in the extracellular space are converted to NAD^+ through the routes described above once entered the cell.

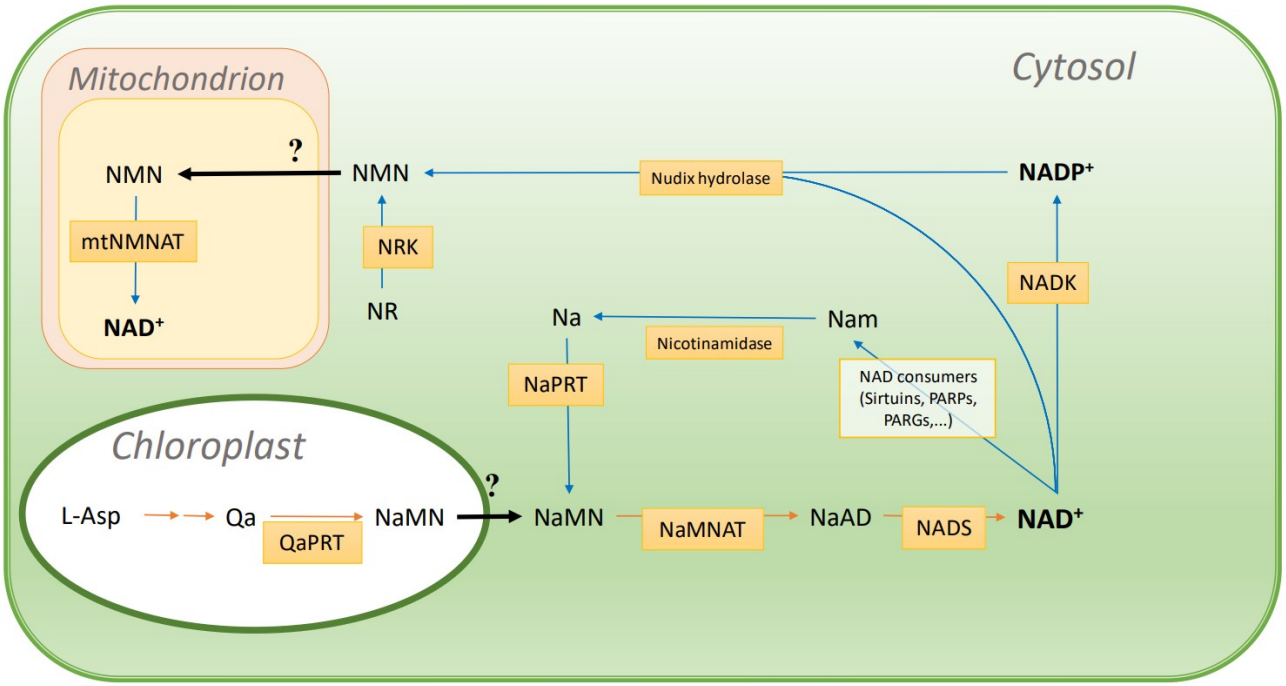

Figure 2. Main NAD^+ metabolic routes in dicotyledons. Figure has been obtained combining information from literature, BLAST and KEGG databases. Orange arrows remark the *de novo* synthesis. Blue arrows remark reactions involved in NAD^+ consumption and recycling pathways. NR: nicotinamide riboside; NRK: nicotinamide ribosyl kinase; NMN: nicotinamide mononucleotide; NaMN: nicotinate mononucleotide; NaMNAT: nicotinate/nicotinamide mononucleotide adenylyltransferase; mtNMNAT: mitochondrial nicotinamide mononucleotide adenylyltransferase; L-Asp: L-Aspartic acid; Qa: quinolinic acid; QaPRT: quinolinic acid phosphoribosyl transferase; NaPRT: nicotinate phosphoribosyl transferase; Na: nicotinic acid; Nam: nicotinamide; NaAD: Nicotinate adenine dinucleotide; NADS: NAD^+ synthetase; NAD^+: nicotinamide adenine dinucleotide; NADK: NAD^+ Kinase; $NADP^+$: nicotinamide adenine dinucleotide phosphate.

Despite the key role of NAD^+ in all living cells' metabolism, the genetic and biochemical landscape around NAD^+ in plant is still a matter of investigation (Gerdes et al. 2012). Little is known about the intracellular traffic of NAD^+ and its metabolites. The transport of NAD^+ in *A. thaliana* mitochondria and chloroplasts has been shown to occur via NDT1 and NDT2 receptors (de Souza Chaves et al. 2019; Palmieri et al. 2009), whereas carriers of NAD^+ metabolites are still unknown. In addition, the presence of enzymes involved in NAD^+ biosynthesis in bacteria and mammals, like NMN nucleotidase (converting NMN to NR) and NMN deamidase (deamidating NMN to NaMN), has not been explored in plants. By performing a BLAST search using *E. coli* NMN deamidase sequence as the query (Accession number: AAN81705.1), we found the occurrence of genes which could code for a putative NMN deamidase in *Cichorium endivia*, *Dorcoceras hygrometricum* and *Digitaria exilis* (Accession numbers: KAI3489635.1, KZV15343.1, LR792838.1) (Figure 3). Therefore, it is clear that future studies are warranted to increase our knowledge on plant NAD^+ metabolism.

```
Dorcoceras_hygrometricum      MESVSVPTDAELRVLAQAVAEETLRQRLMLVTAESCSGGWIAKTLTDLPGSSAWFDAGVV          60
E_coli_PncC                   ------MTDSELMQLSEQVGQALKARGATVTTAESCTGGWVAKVITDIAGSSAWFERGFV          54
Cichorium_endivia             ------MTDHELMQLSEIVGLALKQRGATITTAESCTGGWVAKAITDIAGSSAWFERGFV          54
Digitaria_exilis              ------MTDHELMQLSEVVGLALKQRGATLTTAESCTGGWVAKAITDIAGSSAWFERGFV          54
                                    ** **  *:: *.     :   :.*****:***:**.:**: ******: *.*

Dorcoceras_hygrometricum      TYSYEAKQALLGVDPRTLEHSGAASEETALEMVSGALARFGAGVAVAVTGIAGPSGGTPG          120
E_coli_PncC                   TYSNEAKAQMIGVREETLAQHGAVSEPVVVEMAIGALKAARADYAVSISGIAGPDGGSEE          114
Cichorium_endivia             TYSNEAKAQMIGVRESTLEQHGAVSEPVVIEMAIGALKEARADYAISISGIAGPDGGSDV          114
Digitaria_exilis              TYSNEAKAQMIGVRESTLEQHGAVSEPVVIEMAIGALKEARADYAISISGIAGPDGGSDV          114
                              *** ***  ::**   ** : **.** ..:**. ***    *. *::::*****.**:

Dorcoceras_hygrometricum      KPVGTVWIAWKRRGGYAHAQLFHFDGDREAVRRRTVAAALAGLRKTLTE--        169
E_coli_PncC                   KPVGTVWFAFATARGEGITRRECFSGDRDAVRRQATAYALQTLWQQFLQNT        165
Cichorium_endivia             KPVGTVWFGFATSKGEGITRRECFSGDRESVRRQATVYALKTLWQQFLQNT        165
Digitaria_exilis              KPVGTVWFGFATARGEGITRRECFSGDRESVRRQATVYALKTLWQQFLQNT        165
                              *******:.:    * . ::   *.***::***::.. **  * : : :
```

Figure 3. Sequence alignment of *E. coli* NMN deamidase (PncC, yellow) and putative NMN deamidase in plants. The sequence alignement was generated by Clustal Omega algortithm.

1.3. NAD^+ signalling in plants

Extracellular NAD^+ ($eNAD^+$) has been discovered as a signalling molecule and, in particular, as a trigger of plant's defence mechanisms, able to stimulate transcription of the Pathogen Related Genes (PRGs) and to induce the systemic acquired resistance (Zhang and Mou 2009; Van Loon and Van Strien 1999).

It is normally accepted that when a plant gets an infection, many extracellular signalling molecules deriving from the damaged cells increase their concentration around the infection site. These molecules are collectively known as DAMPs (Damage Associated Molecular Patterns). DAMPs

share the ability to trigger PRGs expression in order to firstly defend the host at a local level. In a second step, they are translocated in the whole infected host, triggering the same genes' expression. As result, a general increase of the entire plant's immunity system will occur. Moreover, DAMP action in reproductive organs will ensure a transgenerational transmission of this immunity through the induction of epigenetic changes (Choi et al. 2014).

Several publications, have addressed the role of $eNAD^+$ as a DAMP, focusing on its involvement in plant resistance against abiotic and biotic stress. The first evidence of NAD^+ involvement in the stress response dates back to 1968 when alterations in $NAD(P)^+$ pool concentrations and subcellular localization have been observed in barley upon *Blumeria graminis* infection (Ryrie and Scott 1968). Subsequent studies in *A. thaliana* showed that stimulation of intracellular NAD^+ biosynthesis increased resistance against *Pst-AvrRpt2*, *Dickeya dadantii*, and *Botrytis cinerea,* likely due to the induction of ROS levels (Pétriacq et al. 2016). It is known that in plants a burst in ROS levels contributes to basal defence in response to both pathogen-associated molecular patterns (PAMPs), which are signals of infection, and DAMPs, which indicate tissue disruption (Pétriacq et al. 2016; Gakière, Fernie, and Pétriacq 2018). More recently, it has been reported that exogenous administration of NAD^+ to *Citrus sinensis* induced resistance to citrus canker caused by *Xanthomonas citri*, indicating that $eNAD^+$ signalling may be conserved in the whole Brassicaceae family (Alferez et al. 2018).

The best known biotic stress response in plants is called systemic acquired resistance (SAR). Here, the stimulation of plant resistance mechanisms is mediated by salicylic acid (SA) among other signals, which has the ability to increase the resistance intensity and rapidity during later infections (Veloso et al. 2014). In a recent work, the exogenous administration of NMN in barley cultivars enhances SA-dependent signalling pathway and activates disease resistance against *Fusarium graminearum* (Miwa et al. 2017). Similarly, in *Arabidopsis thaliana*, exogenous $NAD(P)^+$ causes SA accumulation and triggers resistance to *Pseudomonas syringae* (Zhang and Mou 2009).

NAD^+-dependent resistance is not only associated with the induction of SA marker genes but $eNAD^+$ itself was proposed as a "long distance signal" for SAR propagation. The first evidence of $eNAD^+$ role as potential long distance signal in *A. thaliana* SAR induction was reported in 2012. It was shown that transgenic expression of the human NAD^+-hydrolysing enzyme CD38 resulted in a partially compromised induction of SAR (Zhang and Mou 2012). Furthermore, both in *Arabidopsis thaliana* and *Nicotiana benthamiana,* radio-labelled NAD^+ infiltrated in the extracellular space of lower leaves was detected in the upper leaves after 24 hours, suggesting that $eNAD^+$ can be translocated to systemic tissues (Wang et al. 2019).

The molecular mechanism linking $eNAD^+$ to immunity is matter of investigation. Recently, the $eNAD^+$ capability of eliciting PRGs expression in *A. thaliana* was proposed to be due to its binding to the L-type legume-like lectin receptor kinase 1.8. The extracellular domain of this receptor can perceive NAD^+ released in the extracellular space by dying or death cells after a tissue damage or during the infection process. The subsequent signal transduction leads to PRGs expression (Wang et al. 2017).

References

Alferez, F. M., K. M. Gerberich, J. L. Li, Y. Zhang, J. H. Graham, and Z. Mou. 2018. "Exogenous Nicotinamide Adenine Dinucleotide Induces Resistance to Citrus Canker in Citrus." *Front Plant Sci* 9: 1472. https://dx.doi.org/10.3389/fpls.2018.01472.

Choi, J., K. Tanaka, Y. Liang, Y. Cao, S. Y. Lee, and G. Stacey. 2014. "Extracellular Atp, a Danger Signal, Is Recognized by Dorn1 in Arabidopsis." *Biochem J* 463, no. 3 (Nov 01): 429-37. https://dx.doi.org/10.1042/BJ20140666.

de Souza Chaves, I., E. Feitosa-Araújo, A. Florian, D. B. Medeiros, P. da Fonseca-Pereira, L. Charton, E. Heyneke, J. A. C. Apfata, M. V. Pires, T. Mettler-Altmann, W. L. Araújo, H. E. Neuhaus, F. Palmieri, T. Obata, A. P. M. Weber, N. Linka, A. R. Fernie, and A. Nunes-Nesi. 2019. "The mitochondrial NAD+ transporter (NDT 1) plays important roles in cellular NAD+ homeostasis in Arabidopsis thaliana." *Plant J* 100, no. 3 (Nov): 487-504. https://dx.doi.org/10.1111/tpj.14452.

Di Martino, C., and M. L. Pallotta. 2011. "Mitochondria-Localized Nad Biosynthesis by Nicotinamide Mononucleotide Adenylyltransferase in Jerusalem Artichoke (Helianthus Tuberosus L.) Heterotrophic Tissues." *Planta* 234, no. 4 (Oct): 657-70. https://dx.doi.org/10.1007/s00425-011-1428-6.

Emanuelli, M., F. Carnevali, F. Saccucci, F. Pierella, A. Amici, N. Raffaelli, and G. Magni. 2001. "Molecular Cloning, Chromosomal Localization, Tissue Mrna Levels, Bacterial Expression, and Enzymatic Properties of Human Nmn Adenylyltransferase." *J Biol Chem* 276, no. 1 (Jan 05): 406-12. https://dx.doi.org/10.1074/jbc.M008700200.

Gakière, Bertrand, Alisdair R. Fernie, and Pierre Pétriacq. 2018. " More to NAD+ than meets the eye: A regulator of metabolic pools and gene expression in Arabidopsis" *Free Radic Biol Med* 122 (Jul): 86-95. https://dx.doi.org/10.1016/j.freeradbiomed.2018.01.003.

Gerdes, S, C Lerma-Ortiz, O Frelin, SMD Seaver, CS Henry, V de Crecy-Lagard, and AD Hanson. 2012. "Plant B Vitamin Pathways and Their Compartmentation: A Guide for the Perplexed."

Journal of Experimental Botany 63, no. 15 (SEP 2012): 5379-5395. https://dx.doi.org/10.1093/jxb/ers208.

Hashida, S. N., H. Takahashi, M. Kawai-Yamada, and H. Uchimiya. 2007. "Arabidopsis Thaliana Nicotinate/Nicotinamide Mononucleotide Adenyltransferase (Atnmnat) Is Required for Pollen Tube Growth." *Plant J* 49, no. 4 (Feb): 694-703. https://dx.doi.org/10.1111/j.1365-313X.2006.02989.x.

Helman, T., and N. Braidy. 2022. "Importance of Nad+ Anabolism in Metabolic, Cardiovascular and Neurodegenerative Disorders." *Drugs Aging* (Dec 13). https://dx.doi.org/10.1007/s40266-022-00989-0.

Hunt, L., M. J. Holdsworth, and J. E. Gray. 2007. "Nicotinamidase Activity Is Important for Germination." *Plant J* 51, no. 3 (Aug): 341-51. https://dx.doi.org/10.1111/j.1365-313X.2007.03151.x.

Hunt, L., F. Lerner, and M. Ziegler. 2004. "Nad - New Roles in Signalling and Gene Regulation in Plants." *New Phytol* 163, no. 1 (Jul): 31-44. https://dx.doi.org/10.1111/j.1469-8137.2004.01087.x.

Katahira, R., and H. Ashihara. 2009. "Profiles of the Biosynthesis and Metabolism of Pyridine Nucleotides in Potatoes (Solanum Tuberosum L.)." *Planta* 231, no. 1 (Dec): 35-45. https://dx.doi.org/10.1007/s00425-009-1023-2.

Katoh, A., and T. Hashimoto. 2004. "Molecular Biology of Pyridine Nucleotide and Nicotine Biosynthesis." *Front Biosci* 9 (May 01): 1577-86. https://dx.doi.org/10.2741/1350.

Katoh, A., K. Uenohara, M. Akita, and T. Hashimoto. 2006. "Early Steps in the Biosynthesis of Nad in Arabidopsis Start with Aspartate and Occur in the Plastid." *Plant Physiol* 141, no. 3 (Jul): 851-7. https://dx.doi.org/10.1104/pp.106.081091.

Lebiedzińska, A., and P. Szefer. 2006. "Vitamins B in Grain and Cereal–Grain Food, Soy-Products and Seeds", *Food Chemistry*, vol. 95, issue 1, https://doi.org/10.1016/j.foodchem.2004.12.024.

Lee, C. F., J. D. Chavez, L. Garcia-Menendez, Y. Choi, N. D. Roe, Y. A. Chiao, J. S. Edgar, Y. A. Goo, D. R. Goodlett, J. E. Bruce, and R. Tian. 2016. "Normalization of Nad+ Redox Balance as a Therapy for Heart Failure." *Circulation* 134, no. 12 (Sep 20): 883-94. https://dx.doi.org/10.1161/CIRCULATIONAHA.116.022495.

Matsui, A., and H. Ashihara. 2008. "Nicotinate Riboside Salvage in Plants: Presence of Nicotinate Riboside Kinase in Mungbean Seedlings." *Plant Physiol Biochem* 46, no. 1 (Jan): 104-8. https://dx.doi.org/10.1016/j.plaphy.2007.10.008.

Miwa, A., Y. Sawada, D. Tamaoki, M. Yokota Hirai, M. Kimura, K. Sato, and T. Nishiuchi. 2017. "Nicotinamide Mononucleotide and Related Metabolites Induce Disease Resistance against Fungal Phytopathogens in Arabidopsis and Barley." *Sci Rep* 7, no. 1 (07 25): 6389. https://dx.doi.org/10.1038/s41598-017-06048-8.

Morgan, A. J., and A. Galione. 2008. "Investigating Cadpr and Naadp in Intact and Broken Cell Preparations." *Methods* 46, no. 3 (Nov): 194-203. https://dx.doi.org/10.1016/j.ymeth.2008.09.013.

Palmieri, F., B. Rieder, A. Ventrella, E. Blanco, P. T. Do, A. Nunes-Nesi, A. U. Trauth, G. Fiermonte, J. Tjaden, G. Agrimi, S. Kirchberger, E. Paradies, A. R. Fernie, and H. E. Neuhaus. 2009. "Molecular Identification and Functional Characterization of Arabidopsis Thaliana Mitochondrial and Chloroplastic Nad+ Carrier Proteins." *J Biol Chem* 284, no. 45 (Nov 06): 31249-59. https://dx.doi.org/10.1074/jbc.M109.041830.

Pétriacq, P., J. Ton, O. Patrit, G. Tcherkez, and B. Gakière. 2016. "Nad Acts as an Integral Regulator of Multiple Defense Layers." *Plant Physiol* 172, no. 3 (11): 1465-1479. https://dx.doi.org/10.1104/pp.16.00780.

Ryrie, I. J., and K. J. Scott. 1968. "Metabolic Regulation in Diseased Leaves Ii. Changes in Nicotinamide Nucleotide Coenzymes in Barley Leaves Infected with Powdery Mildew." *Plant Physiol* 43, no. 5 (May): 687-92. https://dx.doi.org/10.1104/pp.43.5.687.

Schippers, J. H., A. Nunes-Nesi, R. Apetrei, J. Hille, A. R. Fernie, and P. P. Dijkwel. 2008. "The Arabidopsis Onset of Leaf Death 5 Mutation of Quinolinate Synthase Affects Nicotinamide Adenine Dinucleotide Biosynthesis and Causes Early Ageing." *Plant Cell* 20, no. 10 (Oct): 2909-25. https://dx.doi.org/10.1105/tpc.107.056341.

Schmeisser, K., and J. A. Parker. 2018. "Nicotinamide-N-Methyltransferase Controls Behavior, Neurodegeneration and Lifespan by Regulating Neuronal Autophagy." *PLoS Genet* 14, no. 9 (Sep): e1007561. https://dx.doi.org/10.1371/journal.pgen.1007561.

Van Loon, LC, and EA Van Strien. 1999. "The Families of Pathogenesis-Related Proteins, Their Activities, and Comparative Analysis of Pr-1 Type Proteins." *Physiological and Molecular Plant Pathology* 55, no. 2 (AUG 1999): 85-97. https://dx.doi.org/10.1006/pmpp.1999.0213.

Veloso, J, T Garcia, A Bernal, and J Diaz. 2014. "New Bricks on the Wall of Induced Resistance: Salicylic Acid Receptors and Transgenerational Priming." *European Journal of Plant Pathology* 138, no. 4 (APR 2014): 685-693. https://dx.doi.org/10.1007/s10658-013-0350-0.

Waller, J. C., P. K. Dhanoa, U. Schumann, R. T. Mullen, and W. A. Snedden. 2010. "Subcellular and Tissue Localization of Nad Kinases from Arabidopsis: Compartmentalization of De Novo Nadp Biosynthesis." *Planta* 231, no. 2 (Jan): 305-17. https://dx.doi.org/10.1007/s00425-009-1047-7.

Wang, C., X. Huang, Q. Li, Y. Zhang, J. L. Li, and Z. Mou. 2019. "Extracellular Pyridine Nucleotides Trigger Plant Systemic Immunity through a Lectin Receptor Kinase/Bak1 Complex." *Nat Commun* 10, no. 1 (10 22): 4810. https://dx.doi.org/10.1038/s41467-019-12781-7.

Wang, C., M. Zhou, X. Zhang, J. Yao, Y. Zhang, and Z. Mou. 2017. "A Lectin Receptor Kinase as a Potential Sensor for Extracellular Nicotinamide Adenine Dinucleotide In." *Elife* 6 (07 19). https://dx.doi.org/10.7554/eLife.25474.

Wang, G., and E. Pichersky. 2007. "Nicotinamidase Participates in the Salvage Pathway of Nad Biosynthesis in Arabidopsis." *Plant J* 49, no. 6 (Mar): 1020-9. https://dx.doi.org/10.1111/j.1365-313X.2006.03013.x.

Wu, Y., J. Kuzma, E. Maréchal, R. Graeff, H. C. Lee, R. Foster, and N. H. Chua. 1997. "Abscisic Acid Signaling through Cyclic Adp-Ribose in Plants." *Science* 278, no. 5346 (Dec 19): 2126-30. https://dx.doi.org/10.1126/science.278.5346.2126.

Yamada, K., J. Lim, J. M. Dale, H. Chen, P. Shinn, C. J. Palm, A. M. Southwick, H. C. Wu, C. Kim, M. Nguyen, P. Pham, R. Cheuk, G. Karlin-Newmann, S. X. Liu, B. Lam, H. Sakano, T. Wu, G. Yu, M. Miranda, H. L. Quach, M. Tripp, C. H. Chang, J. M. Lee, M. Toriumi, M. M. Chan, C. C. Tang, C. S. Onodera, J. M. Deng, K. Akiyama, Y. Ansari, T. Arakawa, J. Banh, F. Banno, L. Bowser, S. Brooks, P. Carninci, Q. Chao, N. Choy, A. Enju, A. D. Goldsmith, M. Gurjal, N. F. Hansen, Y. Hayashizaki, C. Johnson-Hopson, V. W. Hsuan, K. Iida, M. Karnes, S. Khan, E. Koesema, J. Ishida, P. X. Jiang, T. Jones, J. Kawai, A. Kamiya, C. Meyers, M. Nakajima, M. Narusaka, M. Seki, T. Sakurai, M. Satou, R. Tamse, M. Vaysberg, E. K. Wallender, C. Wong, Y. Yamamura, S. Yuan, K. Shinozaki, R. W. Davis, A. Theologis, and J. R. Ecker. 2003. "Empirical Analysis of Transcriptional Activity in the Arabidopsis Genome." *Science* 302, no. 5646 (Oct 31): 842-6. https://dx.doi.org/10.1126/science.1088305.

Zhang, X., and Z. Mou. 2009. "Extracellular Pyridine Nucleotides Induce Pr Gene Expression and Disease Resistance in Arabidopsis." *Plant J* 57, no. 2 (Jan): 302-12. https://dx.doi.org/10.1111/j.1365-313X.2008.03687.x.

Zhang, Xudong, and Zhonglin Mou. 2012. "Expression of the Human Nad(P)-Metabolizing Ectoenzyme Cd38 Compromises Systemic Acquired Resistance in Arabidopsis." *Mol Plant Microbe Interact* 25, no. 9 (Sep): 1209-18. https://dx.doi.org/10.1094/MPMI-10-11-0278.

CHAPTER II

OUTLINE OF THE THESIS

The importance of the vitamins of the group B for life, has been established since more than a century ago. The biologically active form of the B3 vitamin, *i.e.,* the coenzyme NAD^+, plays a central role as energy transducer, electron exchanger, enzymatic substrate and signalling molecule. However, only in last decades the interest in NAD^+-related biochemical landscape in plants has considerably increased. NAD^+ metabolism in plants quickly turned out to be a complex network, impacting not only the core intracellular plant biochemistry pathways (photosynthesis, respiration,…), but also developmental processes at a systemic level such as seed germination, reproduction, and the adaptation to several types of stresses, with a particular role in plant immunity.

The work of this thesis aims to shed light on the role of NAD^+ in plants, both intracellularly and in the extracellular space. The activity research focused on two proteins from *A. thaliana*, an universally accepted model for plants, and in particular for dicotyledons.

In the first part of this PhD dissertation, described in chapter III, we provide a complete characterization of a key enzyme of NAD^+ biosynthesis, NaMN/NMN adenylyltransferase, which catalyses a reaction common to both *de novo* and salvage pathways, thus unifying all NAD^+ biosynthetic routes and influencing the whole plant NAD^+ metabolism.

In the second part of the thesis, reported in chapter IV, we describe the production of a recombinant form of the extracellular domain of the *A. thaliana* lectin receptor kinase 1.8. This transmembrane receptor is highly affine and specific for NAD^+ and its interaction with extracellular NAD^+ promotes transcription of several immune effectors. The availability of the recombinant extracellular domain would be instrumental to its structural characterization. Considering the ability of the receptor to specifically sense the extracellular NAD^+, the structure of the receptor in complex with NAD might shed light on the molecular mechanism underlying its function and might represent a step forward in understanding how NAD^+ fulfills its role as a signaling molecule in plants.

CHAPTER III

MOLECULAR AND STRUCTURAL CHARACTERIZATION OF *A. thaliana* NaMN/NMN ADENYLYLTRANSFERASE

1. INTRODUCTION

1.1. NaMN/NMN adenylyltransferases overview

NaMN/NMN adenylyltransferases (NaMN/NMN-AT) are globular alpha/beta enzymes which transfer the adenylic moiety of ATP onto NaMN or NMN, releasing pyrophosphate (PPi) and producing NaAD or NAD, respectively:

$$NaMN + ATP \rightleftharpoons NaAD + PPi$$

$$NMN + ATP \rightleftharpoons NAD + PPi$$

As reported in Chapter I, in plant NAD^+ can be synthetized both *de novo* and through different salvage pathways that recycle back to NAD^+ the products of its consumption or transform into NAD^+ the extracellularly available vitamins Nam, Na and NR. As shown in Figure 1, by catalysing its reaction the enzyme NaMN/NMN-AT, unifies all NAD biosynthetic routes and is therefore essential for NAD biosynthesis.

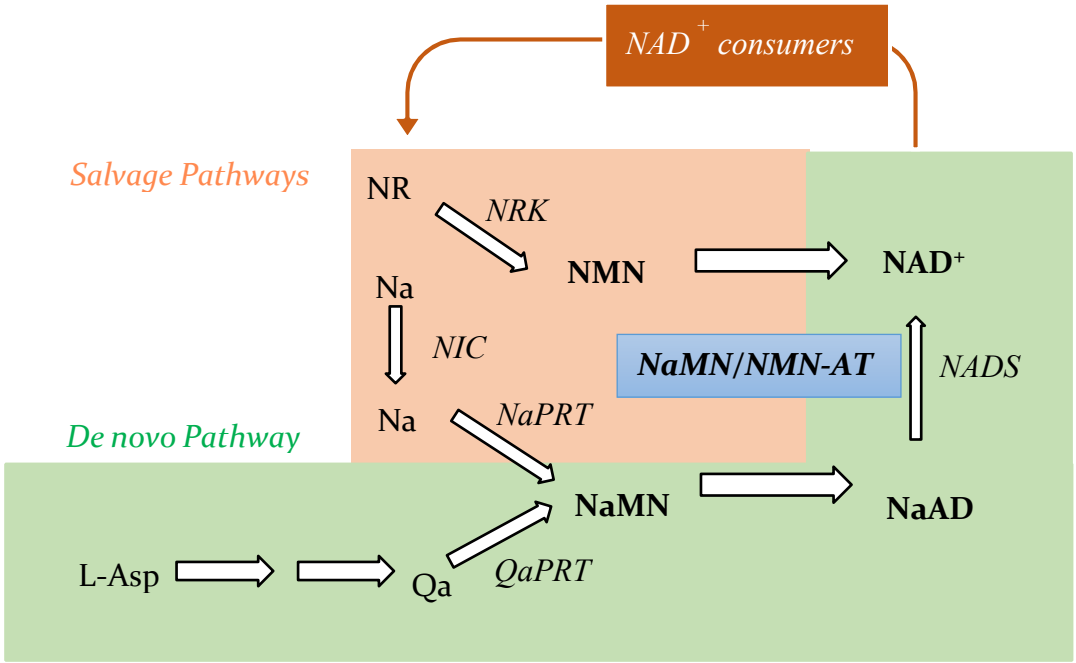

Figure 1. NaMN/NMN-AT unifies all NAD^+ biosynthetic routes. NR: nicotinamide riboside; NRK nicotinamide ribosyl kinase, NMN: nicotinamide mononucleotide, NaMN: nicotinate mononucleotide; NIC: nicotinamidase; NaMN/NMN-AT: nicotinate/nicotinamide mononucleotide adenylyltransferase; L-Asp: L-Aspartic acid; Qa: quinolinic acid; QaPRT: quinolinic acid phosphoribosyl transferase; NaPRT: nicotinate phosphoribosyl transferase; Na: nicotinic acid; Nam: nicotinamide; NaAD: Nicotinate adenine dinucleotide; NAD^+: nicotinamide adenine dinucleotide.

The first NaMN/NMN-AT structure has been solved in 2000 by D'Angelo et al. from the archaebacterium *Methanococcus jannaschii* (D'Angelo et al. 2000). The enzyme was found to share a significant sequence similarity with the *Sulfolobus solfataricus* protein, also displaying the same

thermophilic properties and non-linear kinetic behaviour. It showed a strict preference for the substrate NMN (Magni et al. 2004). In the following years the scientific community focused its attention also on bacterial homologues, with the aim of characterizing a target for antibacterial drugs, since the enzyme catalyses an essential step in NAD biosynthesis. Bacterial enzymes endowed with NaMN/NMN-AT activity are coded by different genes and are typically distinguished in three families: NadD, NadR and NadM. While NadD enzymes show a strict preference for NaMN and are the predominant forms in bacteria, NadR and NadM enzymes are specific for NMN and are present only in some taxonomic groups (Lau, Niere, and Ziegler 2009). In particular, NadR proteins occur in some Gram-negative bacteria and are multifunctional proteins, endowed with both NMNAT and NRK activities, the latter responsible of the phosphorylation of NR to NMN (Raffaelli et al. 1999b; Kurnasov et al. 2002). In addition, in some species, NadR also act as transcriptional repressors of NAD biosynthetic genes through direct binding to DNA (Foster, Holley-Guthrie, and Warren 1987). The *NadM* gene has been found in cyanobacteria, some archaea and some Gram-negative bacteria like *Francisella tularensis*. NadM proteins are also bifunctional enzymes, endowed with NMNAT and ADP ribose pyrophosphatase activities, the latter responsible of the hydrolysis of ADP-ribose, a NAD catabolite, to AMP and ribose-5-phosphate (Lau, Niere, and Ziegler 2009; Raffaelli et al. 1999a). Albeit sharing a strict preference for NaMN, similar substrate's binding site and overall tertiary structure, bacterial NadD enzymes exhibit a different oligomeric assembly depending on the bacterial species. In particular, in Gram-negative bacteria, such as *E. coli* and *P. aeruginosa,* the enzyme exhibits a monomeric structure (Zhang et al. 2002; Yoon et al. 2005), whereas in Gram-positive, e.g. *B. subtilis* and *S. aureus*, the enzyme is a dimer (Olland et al. 2002; Han et al. 2006) and in *Mycobacterium tuberculosis* it shows a tetrameric structure (Rodionova et al. 2015).

In 2002, the structure of the first isoform of the human enzyme (hNMNAT1) has been solved (Garavaglia et al. 2002; Werner et al. 2002; Zhou et al. 2002) and a second isoform (hNMNAT2) has been identified (Raffaelli et al. 2002). The following year, the Zhang group characterized the third isoform (hNMNAT3) for the first time (Zhang et al. 2003). Differently from the enzyme of bacterial NadD family, which are strictly specific for NaMN, hNMNATs either show a higher specificity towards NMN, like hNMNAT1-2, or have a similar catalytic efficiency for both substrates, like hNMNAT3. The three isoforms differ for oligomeric state, intracellular localization and tissue distribution. In particular, hNMNAT1 is a nuclear hexameric enzyme widely distributed in all tissues (Schweiger et al. 2001; Emanuelli et al. 2001); hNMNAT2 is monomeric and has been found on the cytosolic surface of Golgi apparatus of brain, heart, skeletal muscle and beta-pancreatic cells (Lau et al. 2010; Yalowitz et al. 2004); finally, hNMNAT3 is a tetramer that can translocate from cytosol into the mitochondrion and into the lysosome. It is expressed only in few tissues, including lung,

spleen, kidney, and placenta (Berger et al. 2005). Several studies have pointed out the critical role that human NMNATs play in pathological states which are characterized by a decrease of the enzyme activity. For this reason their characterization gained importance for the treatment of cancer, neurodegeneration, retinal disease, erythromelalgia and Alzheimer (Chiang et al. 2012; Gilley and Coleman 2010; Huppke et al. 2019; Jayaram, Kusumanchi, and Yalowitz 2011; Liu et al. 2007; Sorci et al. 2007).

Nowadays, more than 60 3D structures of NaMN/NMN-AT homologues are available in the Protein Data Bank, both in their apoenzymatic form and in complex with different ligands (Table 1).

PDB ID	Year	Gene names	Organism	Resolution (Å)
		ARCHAEA		
1F9A	2001	NadD	Methanococcus jannaschi	2.0
1HYB	2001	NadD	Methanothermobacter thermautotrophicus str. Delta H	2.0
1EJ2	2001	NadD	Methanothermobacter thermautotrophicus	1.9
1M8F	2003	NadD	Methanothermobacter thermautotrophicus	2.4
1M8K	2003	NadD	Methanothermobacter thermautotrophicus	3.0
1M8J	2003	NadD	Methanothermobacter thermautotrophicus	2.4
1M8G	2003	NadD	Methanothermobacter thermautotrophicus	2.0
4YP5	2015	NadD	Methanothermobacter thermautotrophicus str. Delta H	2.21
4YP6	2015	NadD	Methanothermobacter thermautotrophicus str. Delta H	1.9
4YP7	2015	NadD	Methanothermobacter thermautotrophicus str. Delta H	2.3
		CYANOBACTERIA		
2QJO	2008	NadM	Synechocystis sp PCC 6803	2.6
		BACTERIA		
1LW7	2002	NadR	Haemophilus influenzae	2.9
1K4K	2002	NadD	Escherichia coli	2.0
1K4M	2002	NadD	Escherichia coli	1.9
1KAM	2002	NadD	Bacillus subtilis	2.1
1KAQ	2002	NadD	Bacillus subtilis	3.2
1YUL	2005	NadD	Pseudomonas aeruginosa	2.0
1YUN	2005	NadD	Pseudomonas aeruginosa	2.0
1YUM	2005	NadD	Pseudomonas aeruginosa	1.7
2H29	2006	NadD	Staphylococcus aureus	2.0
2H2A	2006	NadD	Staphylococcus aureus	2.1
2R5W	2008	NadM	Francisella tularensis	2.3
2QJT	2008	NadM	Francisella tularensis	2.3
2QTM	2008	NadD	Bacillus anthracis	2.4
2QTN	2008	NadD	Bacillus anthracis	2.4
2QTR	2008	NadD	Bacillus anthracis	1.7

3DV2	2008	NadD	Bacillus anthracis	2.3
3E27	2008	NadD	Bacillus anthracis	2.2
3HFJ	2009	NadD	Bacillus anthracis	2.02
3MLA	2010	NadD	Bacillus anthracis	1.75
3MLB	2010	NadD	Bacillus anthracis	1.8
3MMX	2010	NadD	Bacillus anthracis	2.55
3H05	2009	NadD	Vibrio parahaemolyticus	1.65
4WSO	2014	NadD	Burkholderia thailandensis E264	2.05
4X0E	2015	NadD	Mycobacterium tuberculosis H37Rv	2.41
4RPI	2015	NadD	Mycobacterium tuberculosis H37Rv	2.42
4YMI	2016	NadD	Mycobacteroides abscessus ATCC 19977	1.7
5DEO	2016	NadD	Mycobacteroides abscessus ATCC 19977	2.22
5VIR	2017	NadD	Mycobacteroides abscessus ATCC 19977	1.7
5DAS	2016	NadD	Mycobacterium tuberculosis	2.2
5DB4	2016	NadD	Mycobacterium tuberculosis	2.28
4YBR	2016	NadD	Mycobacterium tuberculosis	1.65
4S1O	2016	NadD	Mycobacterium tuberculosis	1.84
6BUV	2019	NadD	Mycobacterium tuberculosis H37Rv	1.86
6KH2	2020	NadD	Escherichia coli NCCP15648	3.04
6KG3	2020	NadD	Escherichia coli NCCP15649	3.08
6GZO	2019	NadR	Lactococcus lactis subsp. cremoris	3.0
6GYE	2019	NadR	Lactococcus lactis subsp. cremoris	2.3
6GYF	2019	NadR	Lactococcus lactis subsp. cremoris	2.7
PROTOZOA				
5LLT	2016		Plasmodium falciparum 3D7	2.2
5LM3	2016		Plasmodium falciparum 3D7	2.5
VERTEBRATE				
1KR2	2002	NMNAT1	Homo sapiens	2.3
1KQO	2002	NMNAT1	Homo sapiens	2.5
1KKU	2002	NMNAT1	Homo sapiens	2.5
1GZU	2002	NMNAT1	Homo sapiens	2.9
1KQN	2003	NMNAT1	Homo sapiens	2.2
1NUP	2003	NMNAT3	Homo sapiens	1.9
1NUQ	2003	NMNAT3	Homo sapiens	1.9
1NUR	2003	NMNAT3	Homo sapiens	2.15
1NUS	2003	NMNAT3	Homo sapiens	2.2
1NUT	2003	NMNAT3	Homo sapiens	1.9
1NUU	2003	NMNAT3	Homo sapiens	1.9
5Z9R	2019	Nmnat3	Mus musculus	2.0

Table 1. Available NaMN/NMN-AT 3D structures

Structural and sequence comparisons have revealed a common structural architecture characterized by a core of six parallel β-strands flanked by seven α-helices and connecting loops (Figure 2). All structures contain the Rossman fold, typical of the members of the pyridine nucleotide adenylyltransferase (PNAT) superfamily, which comprises a six-stranded dinucleodide binding motif implicated in catalysis.

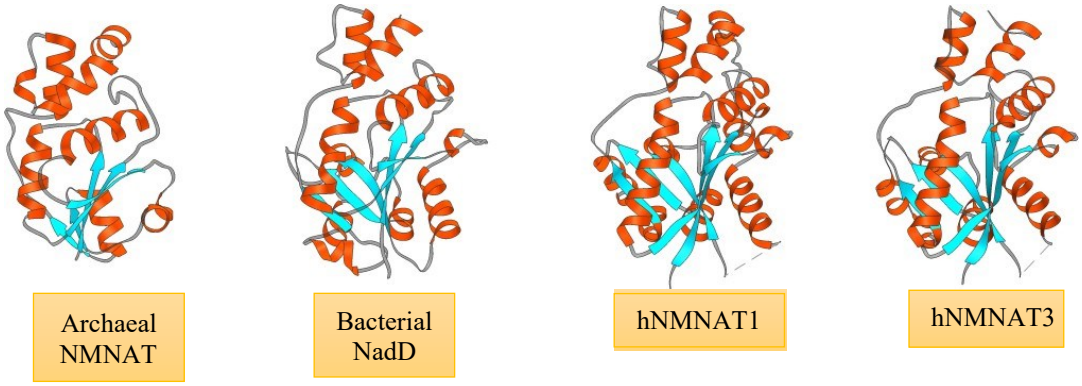

Figure 2. Archaeal NMNAT (PDB ID: 1F9A), bacterial NadD (PDB ID: 1K4K), human NMNAT1 (PDB ID: 1KR2) and hNMNAT3 (PDB ID: 1NUP) monomers have a similar architecture characterized by a core of six parallel β-strands (cyan) flanked by seven α-helices (orange) and connecting loops (grey).

Two conserved fingerprint motifs are considered crucial for ATP binding: the GXFXPX(T/H)XXH motif at the N-terminus and the ISSTXXR sequence at the C-terminus. The identification of these features shared by the whole NaMN/NMN-AT family, combined with kinetic studies, allowed to understand the mechanism of the enzyme's catalysed reaction:

- The nucleophilic 5'-phosphate of NaMN/NMN attacks at the α-phosphate of ATP, whose correct position is determined through interaction with the GXFXPX(T/H)XXH sequence.
- The ATP α-β-phosphates bond is highly bent within the enzyme's active site since the γ-phosphate is kept by the ISSTXXR region.
- Structural magnesium in close proximity to the ATP α-phosphate polarizes the active site and promotes the nucleophilic attack. The ATP α-β-phosphate bond is destabilized and broken, resulting in pyrophosphate released as leaving group.
- The α-phosphate of the AMP moiety and the 5'-phosphate of NaMN/NMN forms the ester bond resulting in formation of NaAD or NAD.

While a random binding of the two substrates has been described for the archaeal enzyme, in human NMNAT1-2 ATP seems to be the first substrate to bind, whereas in hNMNAT3 the pyridine nucleotide is bound first (Sorci, et al. 2007).

1.2 Plant NaMN/NMN adenylyltransferase

In the well-known dicotyledons model organism *Arabidopsis thaliana*, there is only one gene coding for NaMN/NMN-AT (AraAT) (Hunt, Lerner, and Ziegler 2004). The gene is located on chromosome 5 and has been demonstrated to be essential for life, indeed homozygotes organisms lacking both alleles could not be isolated (Hashida, et al. 2007). Many works have been published on the AraAT physiological role in plants: the enzyme was found to be involved in processes like pollen tubes growth, seeds germination, phytopathogens resistance and stomatal guard cells recovery under oxidative stress (Hashida et al. 2010; Hashida, et al. 2007; Miwa, et al. 2017; Wang et al. 2020). Nevertheless, an exhaustive functional and structural characterization of the enzyme is still missing. In 2007 Hashida et al reported a preliminary characterization of recombinant AraAT, expressed in *E. coli* fused with glutathione S-transferase, showing the enzyme's capability to catalyse the production of both NAD^+ and NaAD with comparable efficiency (Hashida, et al. 2007; Hashida, Takahashi, and Uchimiya 2009). The enzyme subcellular location is also an open issue: although many authors have reported NaMN adenylation to occur in the cytosol (Gerdes, et al. 2012; Noctor et al. 2011), in the Uniprot KB database the location of the protein (ID F4K687) was predicted to be nuclear. By using the online server LOCALIZER (Sperschneider et al. 2017), we could predict a cytosolic localization. Furthermore, the presence of an enzyme with a strong preference for NMN in mitochondria from Jerusalem artichokes (Di Martino and Pallotta 2011) suggests the possible existence of splicing variants In this work, an in-depth study of the molecular, functional and structural properties of this key enzyme is provided for the first time, with the aim of expanding the knowledge on NAD^+ biosynthesis in plants.

2. EXPERIMENTAL PROCEDURES

2.1. Cloning, Expression and Purification

The coding sequence of *Arabidopsis thaliana* AraAT, previously cloned into pT7-7 vector, was subcloned into the pET28a vector to allow the expression of a protein with a His-tag at its N-terminus. The recombinant pET28a construct was obtained using In-Fusion® HD Cloning Kit. The pET28a was firstly digested with *Nde*I and *Sal*I restriction enzymes at 37°C for 3 hours. The AraAT coding sequence of 733 bp was then amplified from the recombinant pT7-7 vector, using primers shown in Table 2.

Name	Sequence	Tm°C	CG%	nt	A	T	C	G	Extinction coefficient (1/(mM·cm)	Molecular weight(g/mol)
Fw	5'-cgcggcagccatatggatgtcccgttaccagtc-3'	84.2	60.6	33	6	7	11	9	307.4	10090
Rv	5'-cgcaagcttgtcgactcatgtgagctcagtgtatagttg-3'	79.9	48.7	39	8	12	8	11	372.2	12029

Table 2. Primers for AraAT cloning.

Primers' stability, melting temperature and propensity to dimers formation had been previously assessed through bioinformatic tools. Polymerase Chain Reaction (PCR) was carried out for 30 cycles of denaturation (98°C for 10 sec), annealing (55°C for 10 sec) and extension (72°C for 5 sec). The amplified gene and the linearized vector were incubated with In-Fusion HD Enzyme 5X Premix for 15 minutes at 50°C in a total volume of 10µl mix, in accordance with In-Fusion® kit protocol. The mixture was then transformed into *E. coli* TOP10 F' chemically competent cells and positivity of clones was checked through enzymatic digestion and Sanger sequencing of the plasmids. The obtained recombinant plasmid was purified and transformed into ThermoScientific™ *E. coli* BL21(DE3) Competent Cells. In order to establish the optimal conditions for the expression, the expression level of recombinant AraAT was monitored after 1h, 3h, 5h and overnight incubation after induction of the expression with 1 mM IPTG, at two different temperatures, 25°C and 37°C. Expression occurred in Luria Bertani (LB) medium supplemented with 50 µg/ml kanamycin.

Recombinant AraAT was produced by inoculating an overnight pre-culture of freshly transformed cells into 600 ml of medium. Incubation was performed at 37 °C with rotatory shaking (200 rpm). The expression of the protein was induced with 1 mM IPTG when culture reached an OD_{600} of 0.8. After overnight incubation (18h), induced cells were harvested by centrifugation (6,000 x *g* for 10 min at 4°C). Pellets were stored at -80°C until use. For the protein purification, cells were resuspended in lysis buffer (50 mM HEPES/NaOH pH 7.5, 300 mM NaCl, 10 mM Imidazole, 1 mM PSMF, protease inhibitor cocktail (Sigma®)) and then disrupted with three passages in a French pressure cell (18,000 psi). Crude extract was obtained by removing cells debris with centrifugation (20,000 x *g*, 30 min at 4°C). The recombinant protein was purified at room temperature using Bio-Rad FPLC system equipped with a HisTrap™ FF IMAC column (1ml) with a Nichel-NitriloTriacetic Acid (NiNTA) resin, equilibrated with 50 mM HEPES/NaOH pH 7.5, 300 mM NaCl, 10 mM Imidazole, 2 mM tris-2-carboxyethyl-phosphine. Unbound proteins were removed by washing with 10 column volumes of equilibration buffer, followed by 15 column volumes of equilibration buffer containing 100 mM imidazole. The elution of bound protein was carried out with 15 column volumes of a linear imidazole gradient from 100 mM to 350 mM, in the equilibration buffer. In order to remove imidazole and store the protein, the pool containing the eluted protein, was subjected to a chromatography on a PD-10 desalting column packed with Sephadex G-25 resin, equilibrated and eluted with 50 mM

HEPES/NaOH pH 7.5, 300 mM NaCl, 10 mM Imidazole, 1mM TCEP. Protein was stored at -20°C until use. Purity of AraAT was estimated by 15% SDS-PAGE after staining with Coomassie brilliant blue R-250 (Brunelle & Green, 2014). Protein concentration was determined with Bradford assay, referring to a calibration curve prepared with Bovine Serum Albumin (Bradford, 1976).

2.2. Enzymatic activity determination

2.2.1. Spectrophotometric assay

The enzyme activity was measured in the presence of NMN or NaMN through a spectrophotometric assay coupling NAD^+ or NaAD formation to NADH production.

For the assay of the NMN adenylyltransferase activity, the reaction mixture contained 32 mM HEPES/NaOH pH 7.5, 0.46 % (v/v) Ethanol, 35 mM semicarbazide, 10 mM $MgCl_2$, 0.2 µM alcohol dehydrogenase, 9 µM bovine serum albumin, and appropriate amounts of the enzyme, ATP and NMN. The produced NAD was converted to NADH by alcohol dehydrogenase present in the mixture. The increase of NADH was measured at 340 nm and was used to calculate the activity of the enzyme. 1 Unit of AraAT represents the amount of enzyme that catalyses the synthesis of 1 micromole NAD^+ per minute, at 37°C.

For the assay of the NaMN adenylyltransferase activity, the reaction mixture contained 88 mM HEPES/NaOH pH 7.5, 0.46 % (v/v) Ethanol, 35 mM semicarbazide, 20 mM $MgCl_2$, 0.4 mM NH_4Cl, 0.2 µM alcohol dehydrogenase, 9 µM bovine serum albumin, 0.5 µM NAD^+ synthetase from *Bacillus anthracis* (NadE), and appropriate amounts of the enzyme, ATP and NaMN. In this assay the formation of the product NaAD was coupled to its conversion to NAD^+ and then to NADH by the action of the ancillary enzymes NadE and alcohol dehydrogenase, respectively. The increase of NADH was used to calculate the activity.

2.2.2. HPLC-based assay

The reaction mixture contained 50 mM HEPES/NaOH pH 7.5, 10 mM $MgCl_2$, and appropriate amounts of the enzyme, ATP and NMN or NaMN. Reaction mixtures were incubated at 37°C and catalysis was stopped after 5 and 10 min of incubation by adding $HClO_4$ to a final concentration of 0.6 M. Samples were placed 10 min on ice, and then centrifuged for 2 min at 20,000 x *g*. The supernatants were neutralized with a proper amount of 1 M K_2CO_3, stored at -80°C for 20 min, centrifuged as described above, and injected into a Supelcosil LC18-T column in order to measure NAD^+ or NaAD formation. Products' nature was confirmed by coelution with previously injected standards. Products quantitation was possible through peaks integration. 24 µM cAMP (final concentration) was included in each reaction mixture and was used for peaks areas normalization.

The elution was monitored at 260 nm (Shimadzu SPD-M20A). HPLC analysis have been always performed at 15 °C keeping a flow rate of 1 ml/min. The column was equilibrated with 100 mM KH_2PO_4/KOH pH 6.0, 8 mM tetrabutylammonium hydrogen sulphate (buffer A). Analytes were eluted under the following gradient conditions: 10 min up to 27% buffer B (buffer A plus 30% methanol); 5 min up to 90% buffer B, 3 min hold at 90% buffer B; and 1 min up to 100% buffer A, followed by re-equilibration with buffer A for 7 min.

2.3. Molecular weight determination

Monomeric molecular weight of AraAT was estimated through bioinformatic tools (ProtParam tool from ExPasy, by Swiss Institute of Bioinformatics) and through Rf calculation method on an SDS-PAGE gel. In order to estimate the native molecular weight of AraAT, a gel filtration chromatography was performed through FPLC using a Sephacryl S300 Superfine column (24 ml), equilibrated with 50 mM HEPES/NaOH pH 7.5, 300 mM NaCl. As standard proteins for the generation of the calibration curve monomeric Bovine Serum Albumin (66,430 Da), Ovalbumin (44,287 Da) and Carbonic Anhydrase (29,000 Da) were used.

2.4. Catalytic characterization

NaMN-AT activity was determined by using the HPLC-based assay, at 37°C, in the presence of 1 μM purified enzyme and saturating concentration of NaMN and ATP. Appropriate control mixtures, in the absence of the enzyme, were always processed in parallel. The pH-dependence was measured using citrate at pH 5.0 and 5.5, PIPES at pH 6.0, HEPES at pH 7.0, 7.5 and 8.0 and TRIS at pH 8.5 and 9.0, each buffer at 50 mM final concentration. Optimal temperature was determined at pH 7.5, at temperatures ranging from 4°C to 60°C. Metal ions were tested at 1 mM concentration, at pH 7.5.

2.5. Effect of NAD^+ metabolites

Many NAD^+-derivatives and precursors have been tested for their ability to affect NaAD production catalysed by AraAT. In particular, the effect of NAD^+, $NADP^+$, ADPR, NR, NADH, NADPH at 0.5 mM concentrations was tested in reaction mixtures containing 50 mM HEPES/NaOH pH 7.5, 10 mM $MgCl_2$, 2.35 μM enzyme, 0.015 mM ATP and 0.004 mM NaMN. Incubation was performed at 37°C. The activity was determined by using the HPLC-based assay.

2.6. Kinetic characterization

The kinetic constants of AraAT were calculated for ATP, NaMN and NMN through the HPLC-based assay, maintaining $MgCl_2$ at 10 mM, the pH value at 7.5 and temperature of the reaction at 37°C. Enzyme was fixed at 1.35 μM. Incubation was carried out for an appropriate time ensuring both a

linear increase of product formation with time and a substrate consumption of less than 20%. For the analysis of the NaMNAT-catalyzed reaction, both NaMN and ATP were varied from 5 µM to 60 µM. For the analysis of the NMNAT-catalyzed reaction, NMN was varied from 0.1 mM to 1.5 mM in presence of ATP ranging from 5 µM to 100 µM. The catalytic parameters were calculated by data interpolation with the following equation describing random bi-reactant systems:

$$v = \frac{Vmax \frac{[A][B]}{\alpha K_A K_B}}{1 + \frac{[A]}{K_A} + \frac{[B]}{K_B} + \frac{[A][B]}{\alpha K_A K_B}}$$

In this model, K_A and K_B are the K_m of substrates A and B, respectively. A and B bind randomly, but one substrate can change the dissociation constant for the other one by a factor α. Since the effective K_m for a substrate must be considered at saturating concentration of the other one, the true value of K_m is here represented as the product α x K_m (Segel, 1975).

2.6. Crystallization, Data collection and Structure Determination

Crystals of the apoenzyme were obtained by incubating the pure protein overnight at 4°C with ATP ensuring a molar ratio of 2.5:1 (ligand:protein). The sample was then concentrated using an Amicon Ultra Centrifugal Filter (cut-off 10 kDa, Merck, Millipore) at 4°C, at a final protein concentration of 10 mg/ml. For all AraAT structures in complex with ligands, protein was firstly concentrated to a final concentration between 6 and 8 mg/ml and then incubated for 1 hour at 4°C with ligands at a molar ratio of 50:1 (ligand:protein) before plating. All crystallisation trials were carried out using the sitting drop vapour diffusion method. One microliter of solution of AraAT was mixed with an equal volume of reservoir solution and equilibrated against 100 µl of the reservoir solution. Different commercially available kits were used from JENA Bioscience for the initial screening of crystallization conditions (PACT++, BASIC, Classic HTS I+II and JCSG++ kits). The first crystal was obtained in a reservoir solution containing 100 mM TRIS pH 8.5, 200 mM $MgCl_2$ and 30% (w/v) poly ethylene glycol (Jena Bioscience BASIC kit, condition number C10). Crystals grew to their final size in about two-three weeks at 18°C. Crystallization conditions were consequently optimized and all crystals were observed in the following range of reservoir solutions: 100 mM TRIS pH 8-9, 100-200 mM $MgCl_2$ and 20-40% (w/v) poly ethylene glycol. All crystals were mounted in MiTeGen loops and delivered to the European Molecular Biology Laboratory (EMBL, Hamburg, Germany), beamline P13 for data collection (Cianci et al. 2017). Indexing of the crystallographic dataset images, spots integration, scaling and phasing were performed using MOSFLM (Battye et al., 2011) and XDS/XSCALE program package (Kabsch, 2010).

Crystals belonged to space group $P6_522$ (n°179), with typical unit cells of a=43 Å, b=43 Å, c=430 Å and α=90°, β=90°, γ=120°. Given the sequence of the protein the calculation of the Matthews coefficient and the solvent content indicated one molecule per asymmetric unit. The structure was solved by Molecular replacement using PHASER (McCoy et al. 2007) and one molecule per asymmetric unit was found. The models were checked with the PDB REDO web server (Joosten et al. 2014). An *in silico* model for molecular replacement was obtained using the fold recognition algorithm applied by PHYRE2 (Kelley et al., 2015) and subsequently validated using VADAR (Willard et al., 2003) and MolProbity (Chen et al., 2010) online servers. The manual fitting of the side chains, ligands and solvent molecules into electron density maps was performed using COOT (Emsley & Cowtan, 2004), PHENIX suite {Adams, 2002, PHENIX: building new software for automated crystallographic structure determination}and Refmac5 (Murshudov et al., 1997) of the CCP4 package, under the monitoring of R_{work}, R_{free} and of the Ramachandran plot (Laskowski et al., 1993). Interface areas were calculated with PISA web server (Krissinel and Henrick 2007). Table 3 reports all data collections and refinements statistics.

	apoenzyme	**NMN complex**	**NaMN complex**	**NaAD complex**	**NAD^+ complex**
Wavelength (Å)	0.976	0.976	0.976	0.976	0.976
Space group	P 65 22	P 65 22	P 65 22	P 65 22	P 65 22
Cell parameters (a, b, c, Å)	43.56, 43.56, 435.01	44.04, 44.04, 433.68	43.34, 43.34, 433.50	43.34, 43.34, 433.35	44.08, 44.08, 434.56
Resolution range (Å)	37.73-2.15 (2.227-2.15)	38.14- 1.70 (1.761-1.7)	37.54-2.66 (2.755-2.66)	37.4- 2.6 (2.693-2.6)	38.03- 2.1 (2.175- 2.1) [a]
Total reflections	297304 (14322) [a]	1067415 (54725)	99126 (11721)	187827 (18168)	32126 (3030) [a]
Unique reflections	14722 (1408) [a]	29378 (2827)	7846 (678)	8440 (807)	16063 (1515) [a]
Redundancy	20 (11.5) [a]	36.1 (37.2)	12.4 (12.7)	23.3 (18.2)	34.4 (29.0) [a]
Completeness (%)	99.84 (99.79) [a]	99.89 (99,93)	98.45 (87.93)	99.42 (97.10)	99.83 (99.87) [a]
Mean I/sigma(I)	9.6 (2.2) [a]	27.4 (2.9)	11.7 (1.8)	19.9 (4.1)	14.01 (3.97) [a]
R_{merge} [b]	0.202 (0.769) [a]	0.079 (1.457)	0.139 (1.922)	0.114 (0.705)	0.009 (0.11) [a]
R_{pim} [c]	0.042 (0.218) [a]	0.013 (0.240)	0.041 (0.535)	0.024 (0.168)	0.030 (0.19)
CC1/2	0.996 (0.889) [a]	1.00 (0.954)	1.00 (0.950)	1.00 (0.985)	1.00 (0.970) [a]
CC* [d]	1.00 (0.990)	1.00 (0.988)	1.00 (0.987)	1.00 (0.996)	1.00 (0.992)
Reflections used in refinement	14704 (1405)	29350 (2825)	7816 (610)	8419 (805)	16037 (1513)
Reflections used for R-free	732 (77)	1428 (128)	383 (28)	403 (26)	774 (72)
Wilson B-factor ($Å^2$)	41.58	26.97	66.77	58.63	37.2
R_{work} [d]	0.2212 (0.2264)	0.2103 (0.2270)	0.2546 (0.3137)	0.2264 (0.2832)	0.2000 (0.2092)
R_{free} [d]	0.2586 (0.2802)	0.2358 (0.2839)	0.3100 (0.3117)	0.2666 (0.5299)	0.2473 (0.2695)
Total n. of atoms [d]	1819	2017	1821	1930	2042
macromolecules	1761	1865	1795	1834	1859
ligands	0	23	22	46	89
waters	54	129	25	50	94

ions	4	1	1	1	1
Protein residues	221	235	223	231	234
r.m.s.d. [d]					
bond length (Å)	0.007	0.017	0.002	0.005	0.007
Angles (°)	0.85	1.62	0.48	0.96	0.86
Ramachandran [d]					
favored (%)	96.21	96.54	98.14	95.52	95.18
allowed (%)	3.79	3.46	1.86	4.48	4.82
outliers (%)	0.00	0.00	0.00	0.00	0.00
Average B-factor [d]	45.1	34.06	76.79	66.09	46.29
macromolecules	45.22	34.08	76.86	66.35	45.50
ligands	-	30.86	63.19	101.96	66.73
solvent	40.84	34.26	71.87	60.16	42.51

[a] Values in the highest resolution shell.

[b] $R_{merge} = \sum_{hkl}\sum_j |I_j - \langle I \rangle| / \sum_{hkl}\sum_j I_j$, where I is the intensity of a reflection, and $\langle I \rangle$ is the mean intensityof all symmetry related reflections j.

[c] $R_{p.i.m.} = \sum_{hkl}\{[1/(N-1)]^{1/2} \sum_j |I_j - \langle I \rangle|\} / \sum_{hkl}\sum_j I_j$, where I is the intensity of a reflection, and $\langle I \rangle$ isthe mean intensity of all symmetry related reflections j, and N is the multiplicity. (Weiss, 2001)

[d] Calculated with PHENIX suite (Adams et al., 2002), R_{free} is calculated using 5% of the total reflections that wererandomly selected and excluded from refinement.

jkj

Table 3. Data collection and refinement statistics

2.7. Site-directed mutagenesis

AraAT R106A and R106Q mutants were produced using the commercial kit QuickChange Lightning® (Agilent Technologies, Santa Clara, CA) using primers in Table 4. Positivity of colonies was checked through Sanger sequencing. Mutants were expressed and purified as described for the wild-type enzyme.

Name	Sequence	Tm °C	CG%	nt	A	T	C	G	Extinction coefficient (l/(mM·cm)	Molecular weight(g/mol)
R106A Fw	5'-cttgataaaaccgtcaaagttgcttggtagttgctttgagatgcc-3'	80.9	42.2	45	11	15	8	11	429.8	13881
R106A Rv	5'-ggcatctcaaagcaactaccaagcaactttgacggttttatcaag-3'	80.9	42.2	45	15	11	11	8	437.7	13797
Name	**Sequence**	**Tm °C**	**CG%**	**nt**	**A**	**T**	**C**	**G**	**Extinction coefficient (l/(mM·cm)**	**Molecular weight(g/mol)**
R106Q Fw	5'-cttgataaaaccgtcaaagtttgttggtagttgctttgagatg-3'	77.4	37.2	43	11	16	5	11	419.2	13318
R106Q Rv	5'-catctcaaagcaactaccaacaaactttgacggttttatcaag-3'	77.4	37.2	43	16	11	11	5	419.5	13123

Table 4. Primers used for AraAT mutagenesis.

3. RESULTS AND DISCUSSION

3.1. Production and molecular characterization of the recombinant enzyme

In order to give an insight into NAD^+ plant biosynthesis, we produced AraAT in a recombinant form, as described in Experimental Procedures. In a preliminary experiment, protein expression was monitored both in the cells' debris pellet and in the crude extract of *E. coli* BL21 cells transformed with the recombinant plasmid in order to assess the solubility degree of the expressed protein. As shown in Figure 3, high levels of expression were observed after 3 hours from IPTG addition at both 37°C and 25°C. The protein resulted to be rather soluble, as only a faint band was observed in the cell pellets.

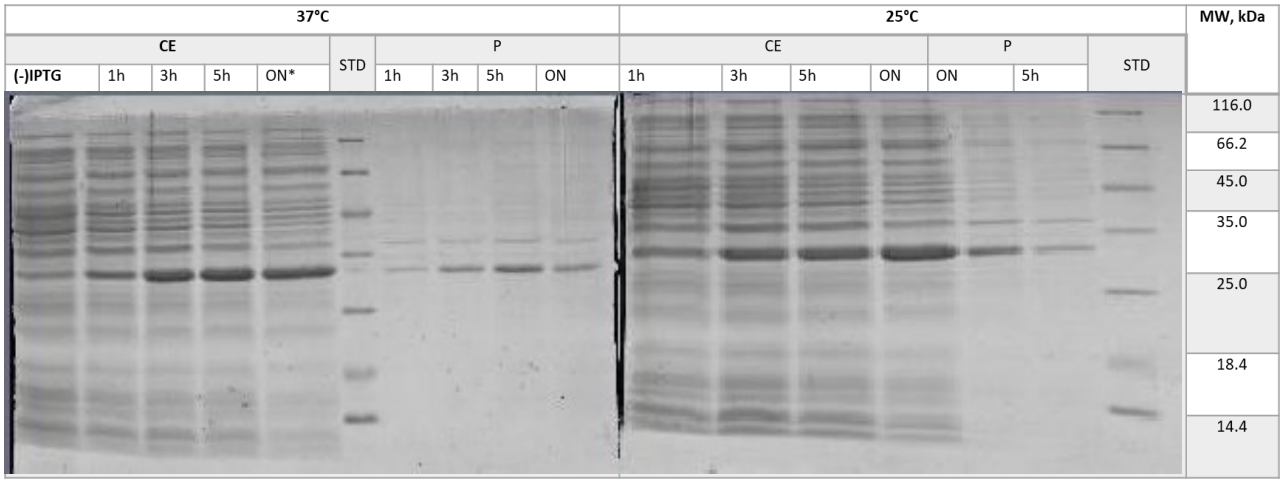

Figure 3. SDS PAGE analysis of crude extracts (CE) and cell pellets (P) at different times after AraAT induction at 37° C (left side) and 25°C (right side).

Recombinant AraAT was purified from the *E. coli* crude extract through Ni^{2+}-chelating affinity chromatography. The NiNTA pool showed half of its original enzymatic activity after an overnight incubation at 4°C, therefore we decided to remove the imidazole through a gel chromatography with Sephadex G-25 resin packed in a PD-10 Desalting Column. The PD10 pool retained the enzymatic activity for at least two weeks at 4°C, and for more than 4 months when stored at -20°C. Purification was checked by subjecting the fractions from the different steps of the procedure to SDS-PAGE analysis (Figure 4).

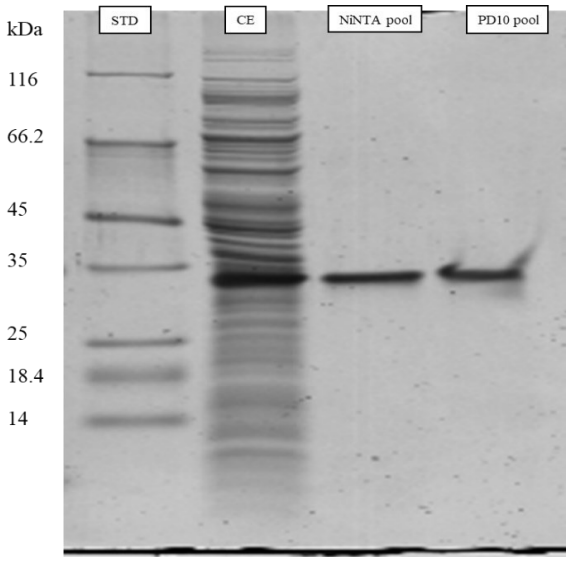

Figure 4. SDS PAGE analysis on a 15% gel of Crude Extract (CE), NiNTA pool and PD10 pool of AraAT purification procedure.

From SDS-PAGE analysis of the pure enzyme we estimated a molecular weight of about 30 kDa. Gel filtration experiments showed a native molecular weight of about 74 kDa (Figure 5). All together the results are consistent with a dimeric structure.

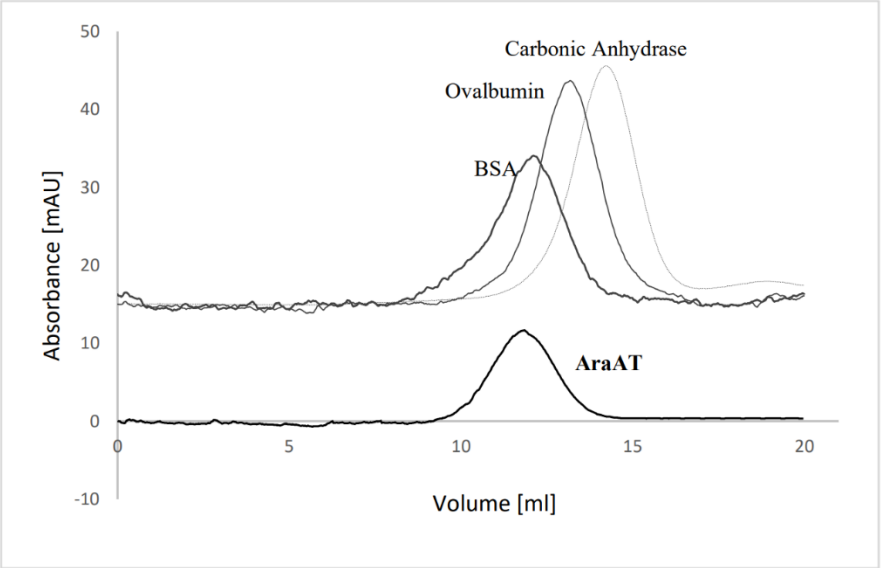

Figure 5. Gel filtration chromatogram of AraAT and standard proteins.

3.2. Catalytic characterization

As shown in Figure 6A, the enzyme was found to be active in a broad range of pH values, with maximal activity between 6 and 7.5. The optimal temperature was at 50°C (Figure 6B).

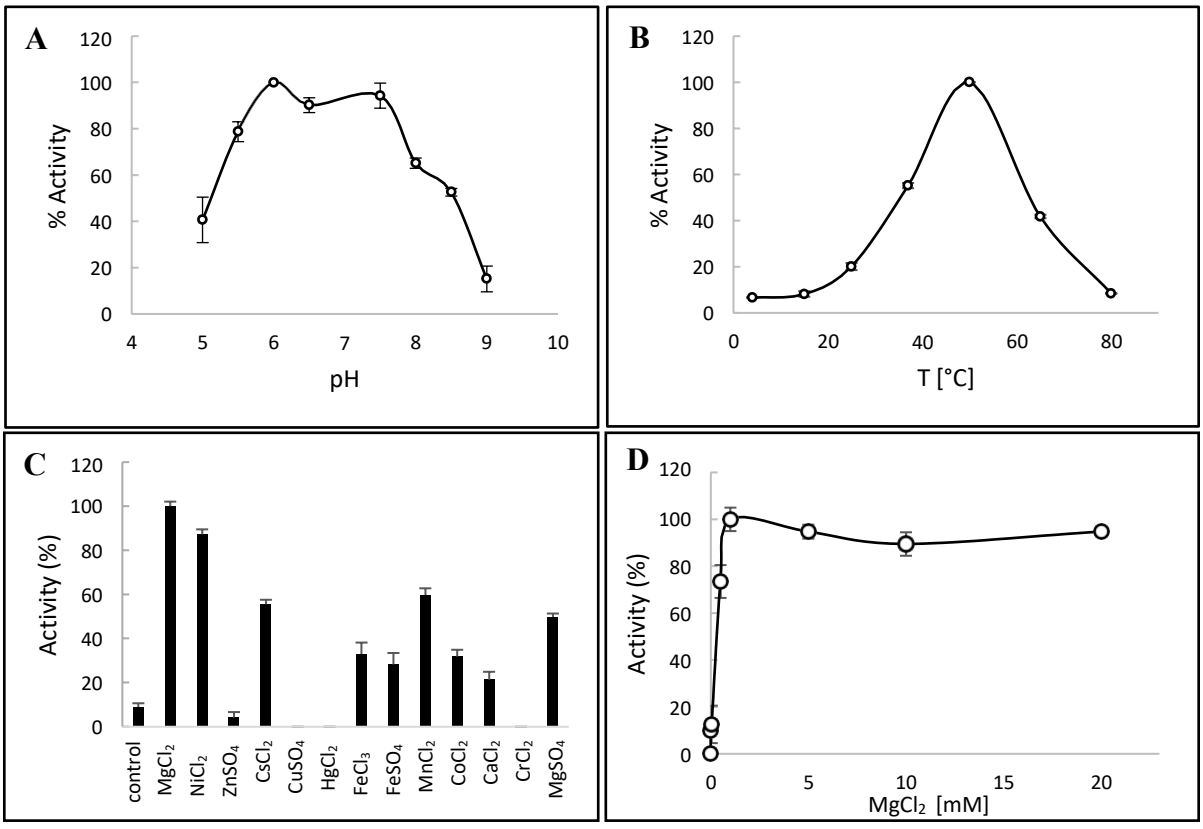

Figure 6. Catalytic characterization of AraAT. (A) Effect of pH on AraAT activity; (B) Effect of temperature on AraAT activity; (C) Metal cofactors dependence for AraAT activity; (D) Effect of $MgCl_2$ on AraAT activity.

Although the optimal temperature for *A. thaliana*'s growth is considered to be about 22-23°C (Pérez-Bueno et al. 2022), a few enzymes, such as acid phosphatase, have shown their highest activity at 50-60°C (Zaman et al. 2022; Zaman et al. 2021; Chafik et al. 2020; Tagad and Sabharwal 2018). This could be a feature of enzymes involved in adapting plant cells to changes in temperatures. In fact, AraAT has been demonstrated to be important in dehydration (Hashida, et al. 2010). Plants can regulate the transpiration and cooling process using specialized leaf pores called stomata, formed by two guard cells, able to change the stomatal aperture. Under high temperatures, cool down process starts through increase of plant transpiration rate and stomata opening. It has been shown that when guard cells mobility is impaired, the expression levels of AraAT significantly increase. At the same time, AraAT overexpressing plant lines showed a higher stomatal response, suggesting a role of the enzyme activity in the correct functioning of guard cells (Hashida, et al. 2010). In this view, AraAT catalytic activity at high temperatures, when the drought risk increases, might guarantee an efficient stomatal movement.

As shown in Figure 6C AraAT seems not to be strictly metal-dependent, as some activity can be measured also in the absence of metal. Among various tested metals, $MgCl_2$ resulted to be the most effective. About 90 % activity was calculated when $MgCl_2$ was replaced by $NiCl_2$ and about 60% of the activity was observed in the presence of $CsCl_2$, $MnCl_2$ and $MgSO_4$. $ZnSO_4$, $CrCl_2$, $HgCl_2$ and $CuSO_4$ resulted to inhibit the enzyme. Figure 6D shows the Mg^{+2}-dependence of the enzyme. Maximal activity was observed at $MgCl_2$ concentrations higher than 1 mM.

Many NAD^+-derivatives and precursors have been tested for their ability to affect AraAT activity. As shown in Figure 7, none of the tested compounds was found to significantly affect the enzyme activity.

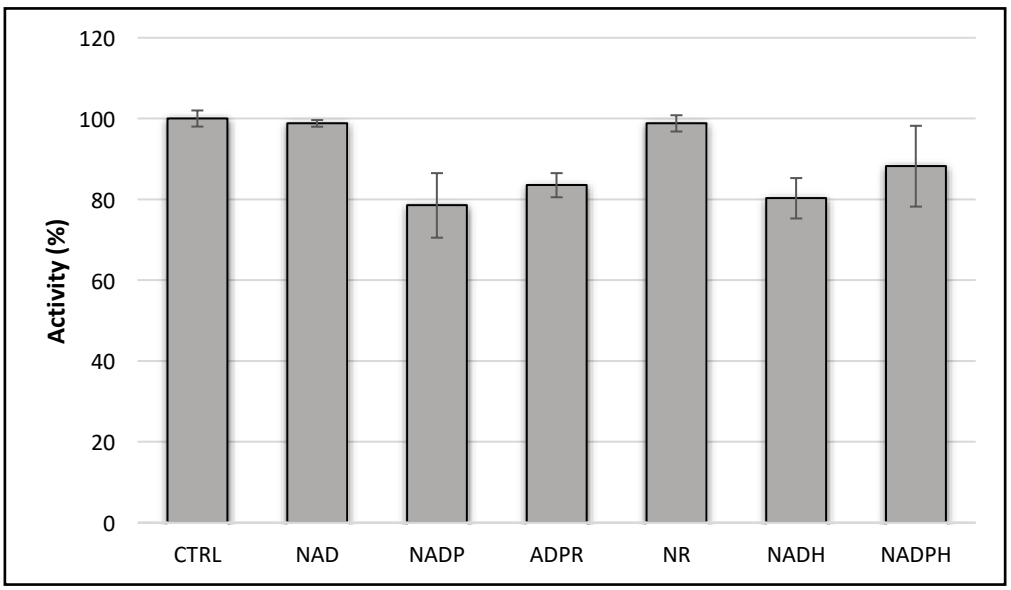

Figure 7. Screening for AraAT effectors.

Kinetic parameters for the NaMNAT- and NMNAT-catalysed reactions were determined as described in Experimental Procedures. Figure 8 shows the double reciprocal plots of NaMNAT kinetics.

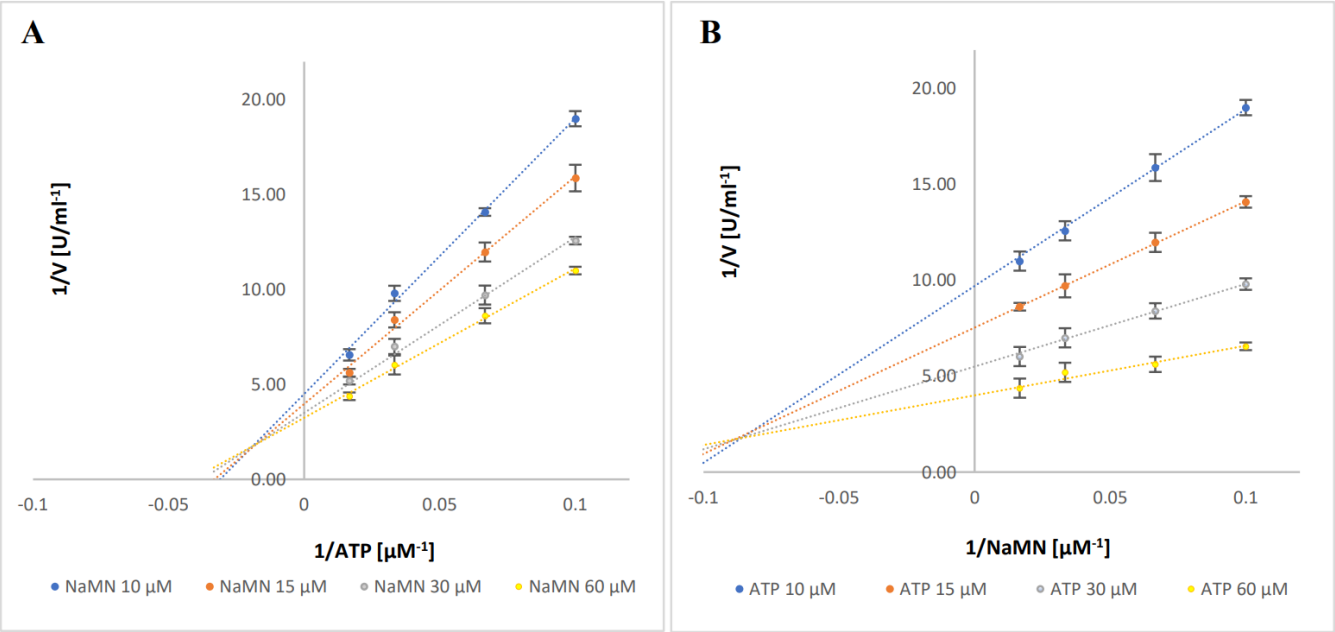

Figure 8. Double reciprocal plots of NaMNAT activity of AraAT measured at (A) ATP and (B) NaMN ranging from 10 to 60 µM.

Initial velocity data of both NaMNAT and NMNAT reactions were found to fit with the equation typical of a random bi-reactant system, involving random binding of the two substrates. This mechanism of reaction is different from that described for yeasts and human NMNATs which show a behaviour consistent with an ordered bi-reactant system (Magni, et al. 2004). Kinetic constants of NaMNAT- and NMNAT-catalysed reactions of AraAT are summarised in Table 5.

Substrate	αK_m [µM]	Vmax [U/mg]	Substrate specificity
$ATP_{(NaMN)}$	23.80±5.74	5.60±0.38	2.35±0.74 x 10^{-1}
NaMN	4.80±0.39		1.22±0.3
$ATP_{(NMN)}$	180.50±53.88	38.21±0.13	2.12±0.56 x 10^{-1}
NMN	6.15±0.7 x 10^{4}		6.26±0.73 x 10^{-4}

Table 5. Main catalytic parameters of AraAT-catalysed reactions in the presence of NaMN and NMN. Substrate specificity is defined as Vmax/αK_m ratio.

Similarly to NMNATs from other sources, AraAT showed K_m values for NaMN and ATP in the micromolar range. Notably, the K_m for NMN was remarkably higher than the value for NaMN, resulting in a substrate specificity for NMN about 2,000-fold lower than that for NaMN. Therefore, NMN cannot be considered a physiological substrate and the enzyme must be discussed as a NaMNAT, which makes it very similar to the bacterial enzymes of the NadD family (Olland et al. 2002). Bacterial NadD in fact shows an affinity higher for the deamidated substrate than for NMN,

differently from bacterial enzymes of the NadM and NadR families which are strictly NMN-dependent, and eukaryotes NMNATs which can use both substrates with comparable efficiency (Berger, et al. 2005; Olland, et al. 2002).

Our kinetic results are not consistent with data reported in the work of Di Martino and Pallotta, who characterized a NMNAT activity in mitochondria from Jerusalem artichokes. Authors calculated a K_m for NMN of 82 ± 1.05 μM by exogenously adding NMN to isolated mitochondria (Di Martino and Pallotta 2011). Based on the finding that there is only one gene in plants encoding for NMNAT, these results suggest that a mitochondrial splicing variant, which preferentially use NMN, might be present.

3.1. Structural characterization

3.1.1. Structure solution

The crystal structure of AraAT was obtained in the native state and in complex with NaMN and NaAD. Moreover, to shed light on the molecular basis underlying the substrate specificity, we also solved the structures in complex with NMN and NAD^+. All crystals showed a hexagonal-base cylindrical shape, typical of the P 6_522 space group which they belong to.

3.1.2. Structure of the apo-enzyme

The apo-AraAT structure was refined to a R_{work}/R_{free} of 0.2212/0.2586 at 2.15 Å of resolution. Although in the asymmetric unit we found a single chain, bioinformatic analysis with the PISA server detected a dimerization interface of 1108.8 $Å^2$ with a monomer generated by two-fold symmetry axis. This result is consistent with the dimeric structure deduced from gel filtration chromatography. The overall architecture of AraAT monomer is represented by an alpha/beta globular protein containing the double-Rossmann fold typical of all PNAT (pyridine nucleotide adenylyltransferase) family members (Figure 9A) (Lau, Niere, and Ziegler 2009). The two monomers combine so that the quaternary structure has two independent binding pockets oriented in opposite directions, as shown in Figure 9B.

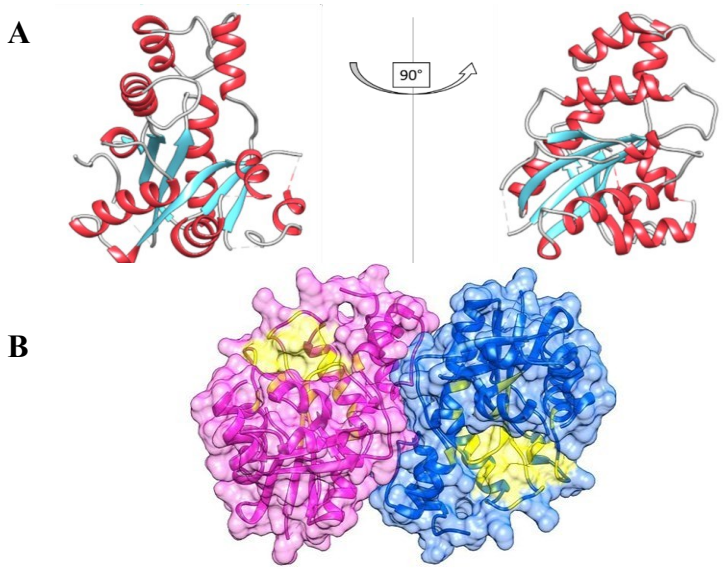

Figure 9. Apo-enzymatic structure. (A) AraAT monomeric structure in ribbon style. α-helixes (red) and β-sheets (cyan) are shown. (B) AraAT dimeric structure in ribbon + surface style. The two chains are coloured in purple and blue. Active sites in each chain are shown in yellow.

Table 6 shows the results of a structural homology search performed by using the DALI server. Values are calculated using backbone atoms. AraAT structural homologues are indicated by their Protein Data Bank identification code and are ordered according to the Z score (Holm 2020). The structure of the AraAT monomer is very similar to that of mammalian NMNAT3 and NMNAT1, followed by the bacterial enzymes of the NadD family. Despite the significant structural homology between the plant and the mammalian enzymes, the proteins exhibit a different quaternary structure. NMNAT3 is a tetramer, whereas NMNAT1 is an hexamer (Schweiger et al. 2001; Zhang et al. 2003).

PDB ID	Protein	Organism	Z score	rmsd [Å]	total residues	%id	residues aligned	%residues aligned
1nur	hNMNAT3	*Homo sapiens*	30.7	1.1	211	43	201	95.26
5z9r	mNmnat3	*Mus musculus*	30.5	1.3	217	41	205	94.47
1kr2	hNMNAT1	*Homo sapiens*	29.9	1.2	233	44	205	87.98
5deo	NadD	*Mycobacterium abscessus*	24	1.8	189	20	186	98.41
5db4	NadD	*Mycobacterium tuberculosis*	23.7	1.6	179	22	176	98.32
2qtr	NadD	*Bacillus anthracis*	22.7	2	189	19	184	97.35
1kaq	NadD	*Bacillus subtilis*	21.8	2.1	186	19	182	97.85
1k4k	NadD	*Escherichia coli*	21.2	2.1	212	20	190	89.62
2h29	NadD	*Staphylococcus aureus*	21	2.2	188	21	180	95.74
1yun	NadD	*Pseudomonas aeruginosa*	20.8	2.4	210	21	192	91.43
4wso	NadD	*Burkholderia thailandensis*	20.8	2.5	227	22	195	85.90
5llt	NadD	*Plasmodium falciparum*	19.2	2.6	205	19	188	91.71
1gn8	Phosphopantetheine adenylyltransferase	*Escherichia coli*	14.9	2.4	159	14	151	94.97
5z1m	Phosphopantetheine adenylyltransferase	*Acinetobacter baumannii*	14.9	2.5	163	15	153	93.87

3x1k	Phosphopantetheine adenylyltransferase	*Pseudomonas Aeruginosa*	14.8	2.5	158	18	150	94.94
7wgj	Phosphopantetheine adenylyltransferase	*Klebsiella pneumoniae*	14.7	2.3	159	14	148	93.08

Table 6. Structural homology search generated with DALI server. AraAT apoenzymatic monomer was used as query and compared against the whole PDB database.

As shown in Figure 10, two fingerprints sequences which are essential for ATP binding and characterize all NMNATs, are conserved in AraAT (Figure 10).

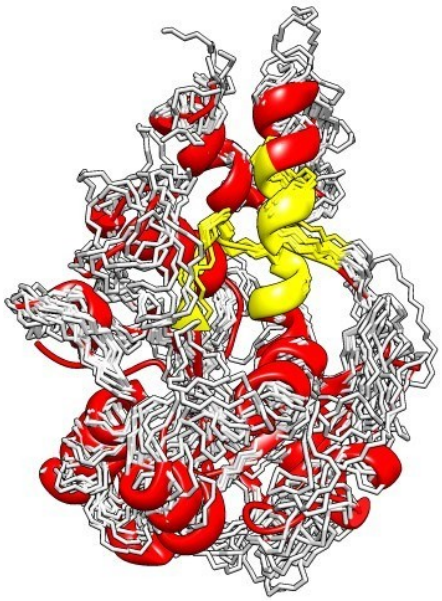

Figure 10. Superimposition of AraAT monomer (red ribbon style) with structural homologues in Table 6 (white backbone chain traces). In the AraAT structure the fingerprints sequences characterizing all NMNATs in conserved positions are coloured in yellow.

Most of the interactions which contribute to AraAT dimerization are H-bonds involving both backbone and sidechains. Structural analysis allowed to identify two loops (88-92 and 213-223) and the alpha-helix α1 (36-51) involved in dimer formation. In particular, Ser 216, Lys 218 and Asp 223 in the loop 213-223 of chain A contact the Arg 40, Glu 43, Asp 47 in α1 and the Ser 89 and Ser 90 in loop 88-92 in chain B. This pattern is repeated identically for the interactions of chain B with chain A (Figure 11).

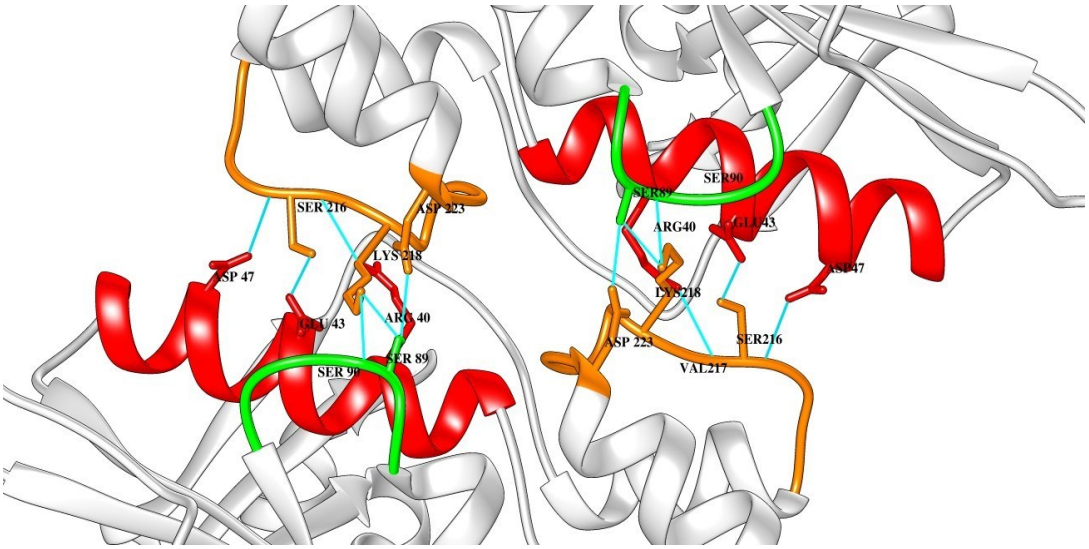

Figure 11. Main interaction involved in AraAT dimer formation. H-bonds (cyan lines) between loop 88-92 (green), loop 213-223 (orange) and α1 helix (red) allow the dimerization.

We found that a similar surface of interaction is present in the hNMNAT1 hexamer and in the hNMNAT3 tetramer (Figure 12).

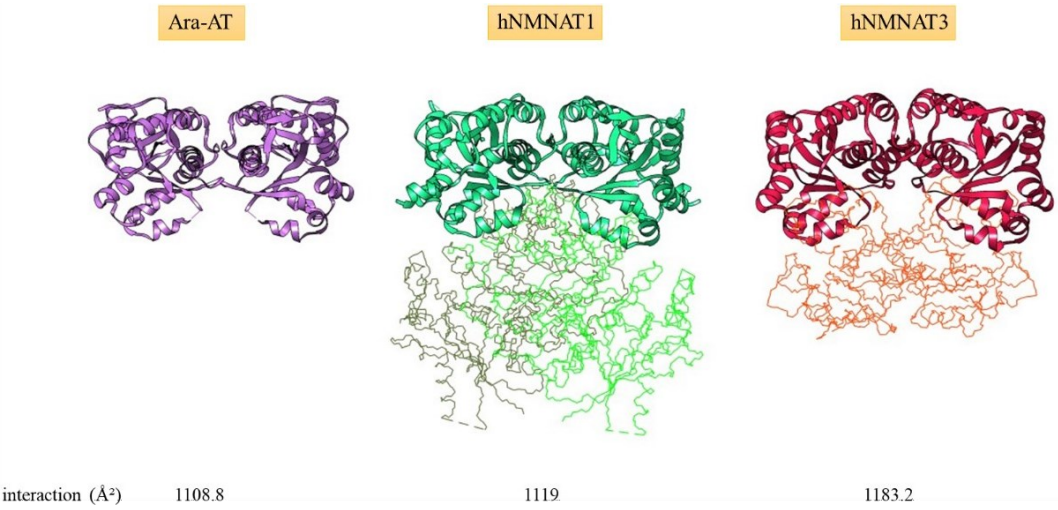

Figure 12. AraAT dimerization interface shares a high degree of similarity with other oligomeric eukaryotic NMNATs. Structural alignment revealed that the dimer formed in AraAT is also present in the hexameric structure of human NMNAT1 (RMSD = 0.81 Å) and in the tetrameric structure of human NMNAT3 (RMSD = 0.97 Å).

3.1.3. Structure of the enzyme in complex with NaMN and NMN

Crystals of the AraAT-NaMN complex diffracted to 2.66 Å resolution. Crystallographic data were processed and the structure was refined as for the apo-enzymatic structure. Structure refinement proceeded up to values of R_{work} and R_{free} of 0.3097 and 0.2544, respectively. Structure of AraAT-

NMN complex reached a resolution of 1.7 Å and refined to values of R_{work} and R_{free} 0.2103 and 0.2358, respectively. Neither for AraAT-NaMN and AraAT-NMN complexes, some conformational changes were detected to occur upon ligand binding. The loop 146-151, not solved in the apo-enzymatic structure, could be modelled, suggesting that it gets closer to the binding pocket, probably because of the Trp 149 interacting with ligands. Furthermore, a general improvement of the backbone electron density signal was observed in all structures compared to apo-AraAT model. Residues of regions 30-38, 165-168 and 190-207, not modelled in the apoenzymatic structure, were partially or completely solved in the other ones.

Superimposition of AraAT apoenzymatic structure with models of AraAT complexed with NaMN and NMN gives a total Root Mean Square Deviation RMSD of 0.417Å (Figure 13).

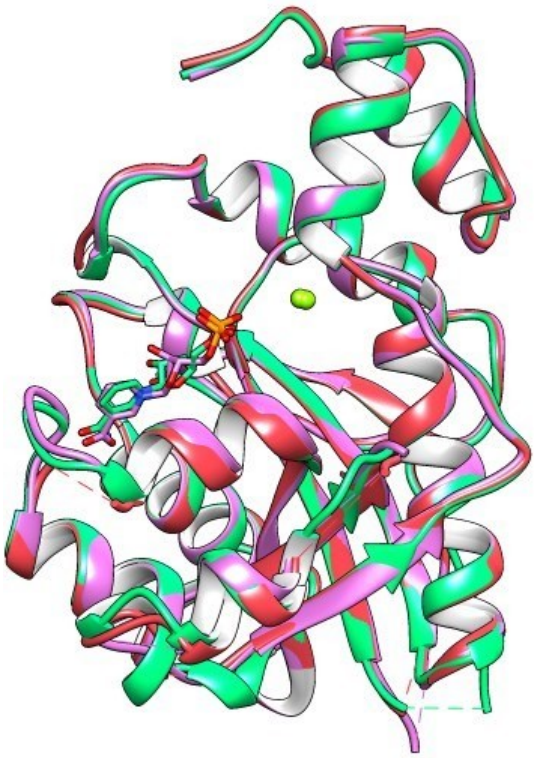

Figure 13. Superimposition of apo-AraAT structure and AraAT (red) complexes with magnesium (light green), NaMN (purple) and NMN (green).

Binding poses of NMN and NaMN appeared strictly comparable and involve common aminoacids: the pyridine ring is pi-stacked between Tyr 104 and Trp 149 and the phosphate group binding is determined by Ser 29. A different ribose orientation is observed in the NMN and NaMN binding poses, since in the NMN-complexed structure hydroxyls point towards the inner part of the pocket and interact with two water molecules (w 18 and w 44, at 2.66 and 2.82 Å of distance, respectively)

absent in the NaMN-complexed structure. An additional difference is in the coordination of amidic and carboxylic group of NMN and NaMN, respectively.

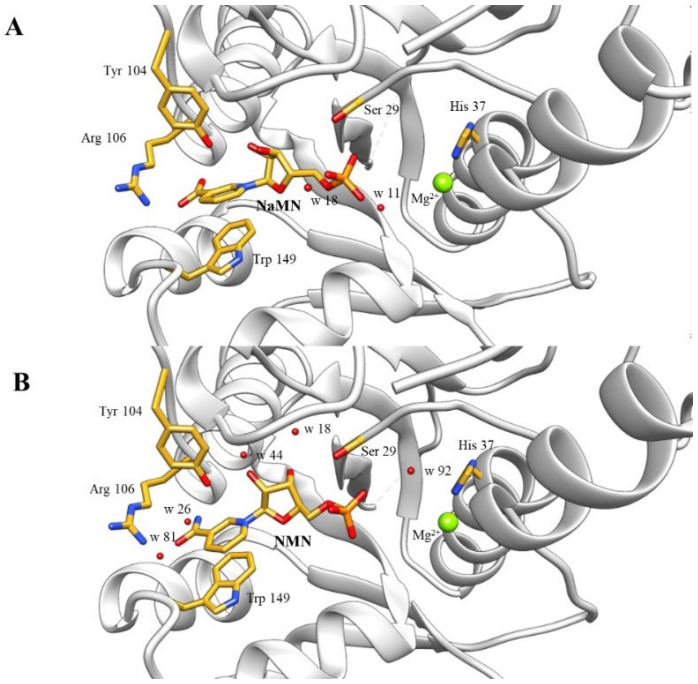

Figure 14. Key interactions in NaMN (A) and NMN (B) complexes.

In fact, the amidic moiety of NMN is H-bound to two water molecules in the active site (w 81 and w 26, distant 2.64 and 2.65 Å, respectively), in proximity to Arg 106. These waters are absent in the NaMN structure and Arg 106 is directly involved in the carboxylic binding through a salt bridge interaction. This would partially explain the preference of AraAT for NaMN in catalysis.

3.1.4. Structure of the enzyme in complex with NaAD and NAD^+

We determined the structures of the enzyme in complex with NaAD and in complex with NAD^+ to map the binding site of AMP moiety. Interestingly, both structures showed a very weak signal in correspondence to the adenine ring of the substrate due to atomic B-factors higher than 100 and occupancies lower than 0.7 in average. This high mobility results in a lower interaction energy and might explain why we were not successful in obtaining protein crystals in complex with ATP. In order to reveal the key residues interacting with the adenylyl moiety of NaAD, we modelled the AMP moiety through polder maps calculation both for NaAD and for those residues in the ligand proximity presenting high B-factor. (Liebschner et al. 2017). The resulting ligand map was more likely to show the omitted atoms than the bulk solvent. Nevertheless the map visualization has been indicative only for a generic adenine ring pose: the low data resolution and the low signal-to-noise ratio made difficult

to understand the exact atomic coordinates. Inspection of other polder maps revealed a certain degree of mobility of the residues in the AMP-side of the binding pocket. In particular we identified two alternate conformations for sidechains of Met 36 and Arg 39 (Figure 15).

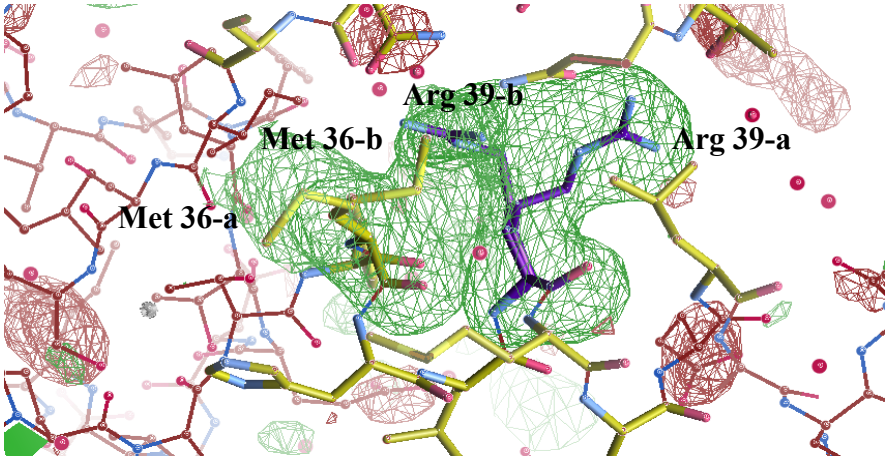

Figure 15. Polder maps (green) for Met 36 (yellow) and Arg 39 (purple). These residues show a double sidechain conformation. Optimal refinement was obtained imposing occupancies for Met 36-a and Met 36-b at 0.67 and 0.33, respectively and Arg 39-a and Arg 39-b at 0.75 and 0.25, respectively.

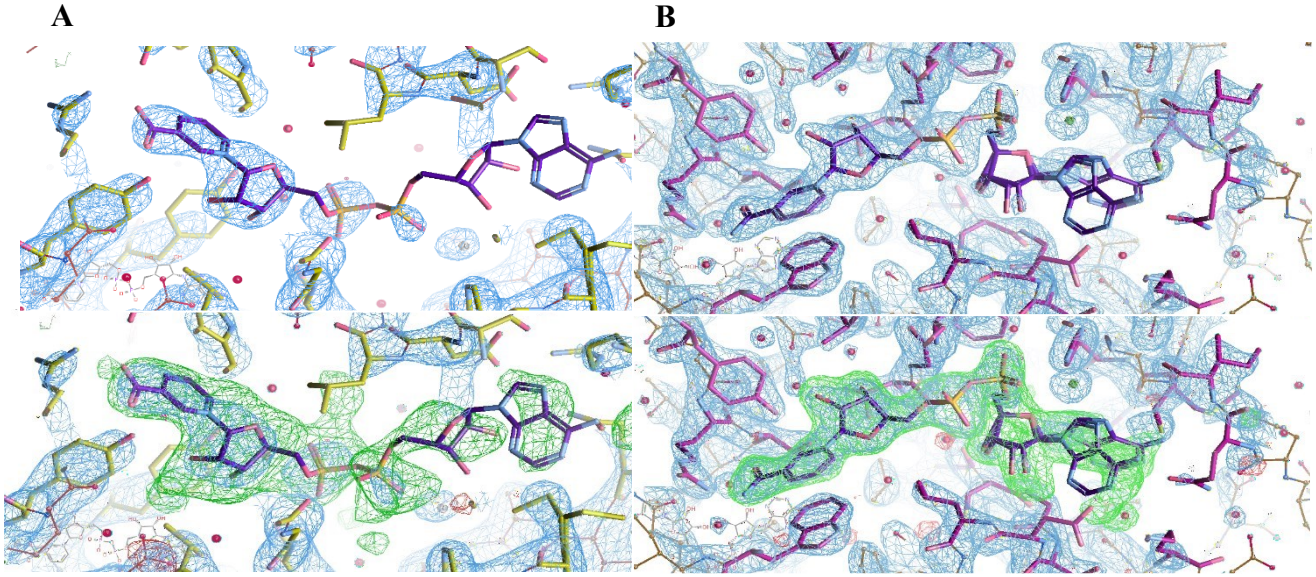

Figure 16. Comparison of 2Fo-Fc map at 1.50 r.m.s.d. (light blue) and Polder maps at 3.00 r.m.s.d. (green) for NaAD (A) and NAD^+ (B).

Crystals with NaAD were solved at a resolution of 2.6 Å and R_{work} and R_{free} were refined up to final values of 0.2264 and 0.2666, respectively. The NaMN moiety of the dinucleotide was found in the same position as in the NaMN-complex and interactions described for NaMN-complex were conserved. Similarly to what observed in NaAD-complex, also in the NAD^+-complex the electron density of the AMP moiety of NAD^+ appeared weak and noisy. The higher resolution of diffraction

(2.1 Å) allowed a better refinement than the NaAD-complex. Final R_{work}/R_{free} values were 0.2000 and 0.2473. Polder maps calculation showed that the NAD^+ atoms signal and the AMP moiety could be modelled with more precision. In particular we repeated the polder map calculation for Met 36 and noticed the same alternate conformation present in the NaAD-complex. The high mobility of environment in the binding pocket proximity might reflect the NAD^+ mobility itself. The two Met 36 conformations (-a and -b) and NAD^+ conformations (-a and -b) were refined imposing occupancy at 0.5 for each and are shown in Figure 17.

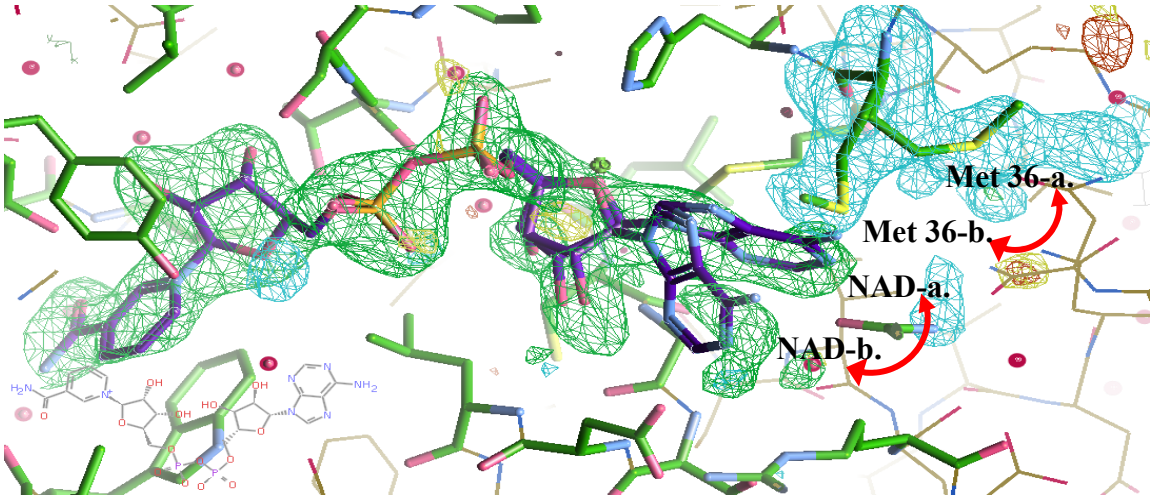

Figure 17. NAD^+ binding pose in AraAT. Polder maps calculation for Met 36 (cyan map) and NAD^+ (green map) revealed two alternative conformation for both residues: Met 36-a and Met 36-b (green); NAD-a and NAD-b (purple).

The NMN moiety of NAD^+ showed the same contact as free NMN. We could report an interaction between the amine moiety of the NAD^+-adenine ring and the Gln 200 sidechain. The Arg 168, conserved in other NMNATs and usually involved in pi-stacking of the adenine ring, here interacts with Asp 138 and does not take part in ligand binding. (Figure 18).

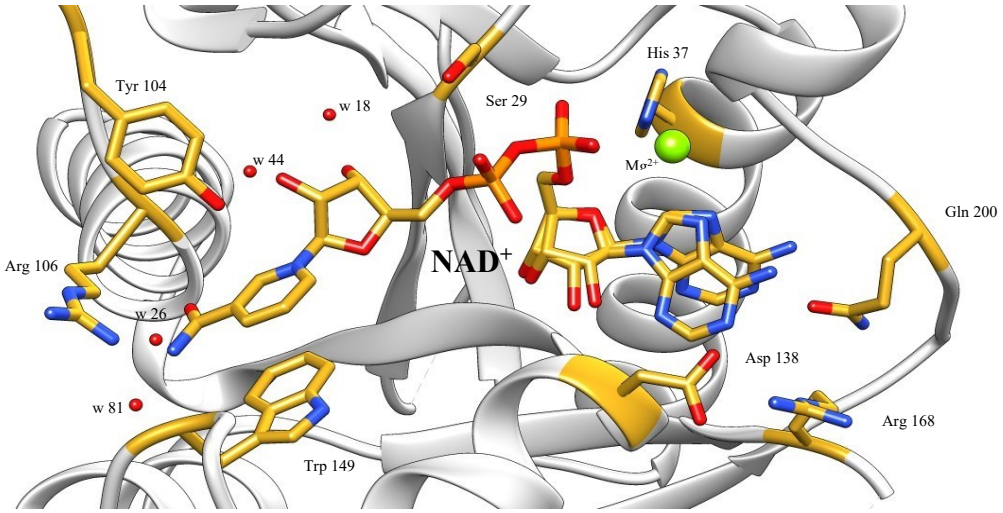

Figure 18. Key interactions of NAD and Mg^{2+} ion in the AraAT binding pocket.

3.3.5. Dual substrate specificity

Structural superimposition of AraAT-NMN and AraAT-NAD^+ complexes with hNMNAT1 and hNMNAT3 (PDB IDs: 1KQN and 1NUU) revealed w 81 and w 26 in our structures to correspond to the structurally conserved water molecules considered crucial in carboxamide coordination (Schweiger, et al. 2001; Lau, Niere, and Ziegler 2009). The fo-fc maps for the NaMN-complex and for NaAD-complex did not show any signal corresponding to w 81 and w 26. For this reason, we can conclude that AraAT binds amidic moieties of NMN and NAD^+ through H-bonds mediated by conserved waters, similarly to human NaMN/NMN-ATs; on the other hand, the enzyme binds the carboxylic groups of NaMN and NaAD through a salt bridge with Arg 106. This interaction is reasonably stronger than H-bonds and could explain the preference of AraAT for the deamidated compound. The position of this residue and the orientation of its sidechain, so close to the amidic/carboxylic atomic coordinates, suggests that it is a key aminoacidic for the specificity of AraAT towards NaMN.

Intrigued from the structural models' inspection, and with the aim to investigate the role of Arg106 in AraAT substrate specificity, we performed a multiple sequences alignment (MSA), comparing many bacterial enzymes of the NadD family and eukaryotic NaMN/NMN-ATs (Figure 19). From this analysis we found that Arg 106 is not strongly conserved: in bacteria, it is mainly substituted by a tyrosine; in human NMNAT1 and 3 it is substituted by a glutamate and in human NMNAT2 by a threonine. Nevertheless, cyanobacterial NadD enzymes from *Synechocystis PCC6803* and *Synechocystis PCC6714* present an arginine, similarly to yeasts NMNAT2, NaMN/NMN-AT in green algae, fungi and higher plants, *A. thaliana* included. This is not surprising considering that cyanobacteria are known as the first photosynthetic organisms as well as chloroplasts ancestors. In this taxon, apart from some exceptions, NMNAT/NaMN-AT might be considered as a NadD ancestor, more affine to a deamidated substrate (Gerdes et al. 2006). It might be that some traits of this enzyme have been conserved in all plant clades.

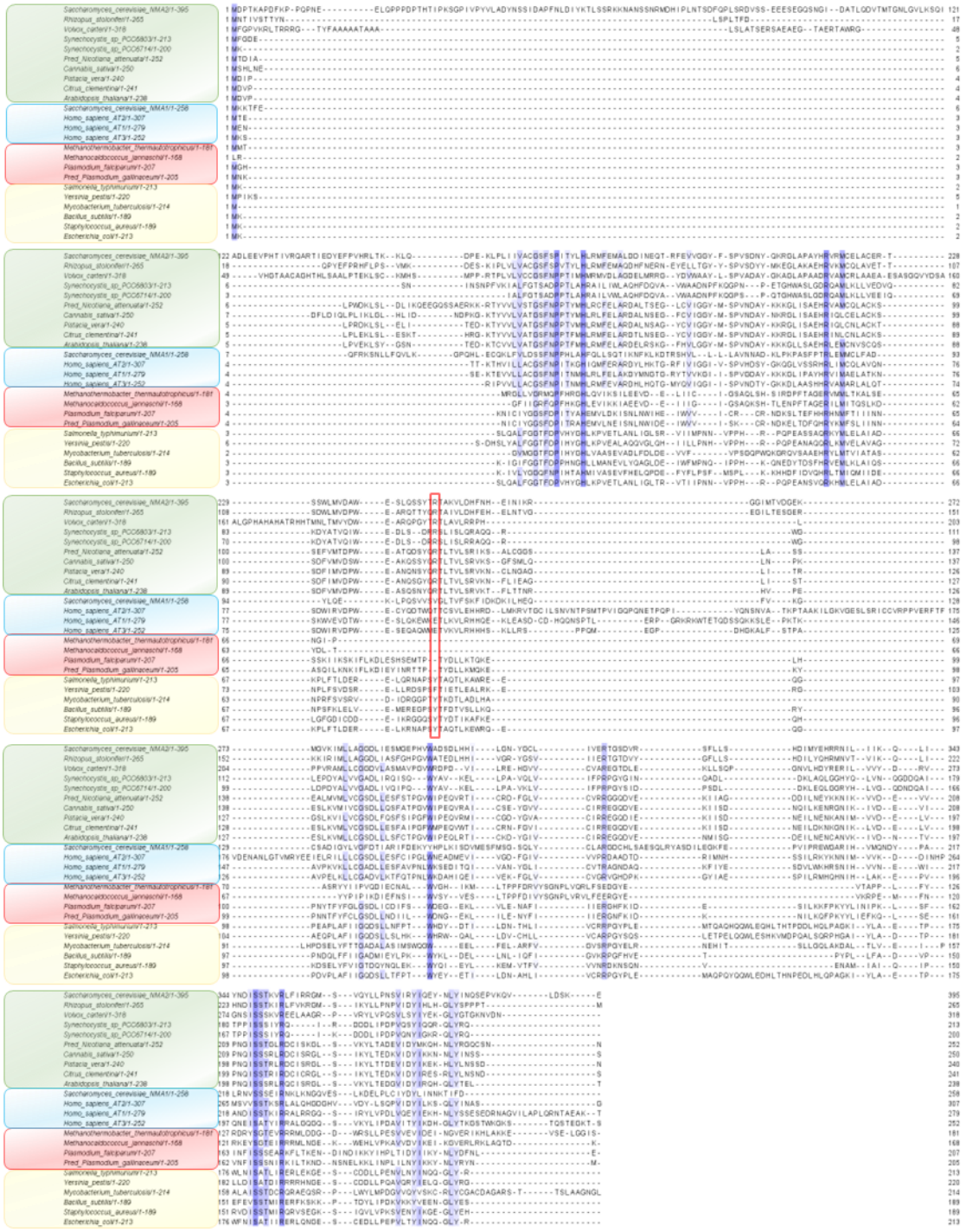

Figure 19. MSA of NaMN/NMN-ATs protein sequences from different sources. The MSA was generated by T-Coffee algortithm and edited using JALVIEW (Clamp et al. 2004), the intensity of blue color increases according to the significance of the BLOSUM62 matrix score, above 30% of conservation. Arginine 106 and the aligned residues are circled in the red box. A phylogenetic tree, generated using Neighbor Joining method, was obtained from the MSA and four groups have been highlighted: (1) higher plants, green algae, fungi, cyanobacteria and the isoform 2 of yeast NMNAT (green box), (2) mammalian and yeast isoform 1 (cyan box), (3) archaea and protozoa (red box) and (4) bacteria (yellow box).

In order to understand the role of the Arg106 in substrate specificity, we produced two mutants of AraAT substituting the arginine with alanine (R106A) and with glutamine (R106Q). The kinetic parameters of the mutated enzymes compared with those of the wild-type are shown in Table 7.

AraAT wild-type			
Substrate	**αK_M [µM]**	**Vmax [U/mg]**	**Substrate specificity**
$ATP_{(NaMN)}$	23.80±5.74	5.60±0.38	2.35±0.74 x 10^{-1}
NaMN	4.80±0.39		1.22±0.3
$ATP_{(NMN)}$	180.50±53.88	38.21±0.13	2.12±0.56 x 10^{-1}
NMN	6.15±0.7 x 10^{4}		6.26±0.73 x 10^{-4}

AraAT R106A			
Substrate	**αK_M [µM]**	**V_{max} [U/mg]**	**Substrate specificity**
$ATP_{(NaMN)}$	2.05±0.56	4.56±0.26	2.22±0.38
NaMN	541.22±8.11		8.42 ±0.25 x 10^{-3}
$ATP_{(NMN)}$	72.58±4.14	52.47±0.74	7.23±0.34 x 10^{-1}
NMN	3.16±1.8 x 10^{4}		1.66±0.16 x 10^{-3}
AraAT R106Q			
Substrate	**αK_M [µM]**	**V_{max} [U/mg]**	**Substrate specificity**
$ATP_{(NaMN)}$	0.47±0.15	6.65±0.78	14.04±4.026
NaMN	369.7±22.5		1.80 ±0.32 x 10^{-2}
$ATP_{(NMN)}$	26.41±2.2	49.12±2.23	1.86±0.14
NMN	1.36±0.15 x 10^{4}		3.61±0.63 x 10^{-3}

Table 7. Comparison of AraAT wild-type, R106A and R106Q catalytic constants.

The V_{max} values of NMNAT- and NaMNAT-catalyzed reactions for both mutants remained of the same order of the wild-type value. However, both R106A and R106Q showed a significant increase of the K_m for NaMN, from 4.8 µM to 541 µM and 370 µM, respectively. In particular, the K_m for NaMN increased of about 90-fold for R106A and of about 60-fold for R106Q. The charge removal in R106A mutant strongly compromised the substrate binding, likewise replacement of the arginine-nicotinate salt bridge by a glutamine dipole interaction, had a strong effect on NaMN affinity. Both mutations did not significantly affect the kinetic parameters towards NMN. These results suggest that Arginine 106 is a key residue for NaMN binding in AraAT. While in bacterial enzymes of the NadD family the substrate specificity is determined by H-bonds with backbone amides of conserved residues (Zhang, et al. 2002) and in eukaryotic NaMN/NMN-ATs it depends on structurally

conserved water molecules (Garavaglia, et al. 2002; Zhang, et al. 2003; Zhou, et al. 2002), in plant enzymes it might be determined by salt-bridge interaction with this conserved arginine.

References

Adams, P. D., R. W. Grosse-Kunstleve, L. W. Hung, T. R. Ioerger, A. J. McCoy, N. W. Moriarty, R. J. Read, J. C. Sacchettini, N. K. Sauter, and T. C. Terwilliger. 2002. "Phenix: Building New Software for Automated Crystallographic Structure Determination." *Acta Crystallogr D Biol Crystallogr* 58, no. Pt 11 (Nov): 1948-54. https://dx.doi.org/10.1107/s0907444902016657.

Battye, T. G., L. Kontogiannis, O. Johnson, H. R. Powell, and A. G. Leslie. 2011. "Imosflm: A New Graphical Interface for Diffraction-Image Processing with Mosflm." *Acta Crystallogr D Biol Crystallogr* 67, no. Pt 4 (Apr): 271-81. https://dx.doi.org/10.1107/S0907444910048675.

Berger, F., C. Lau, M. Dahlmann, and M. Ziegler. 2005. "Subcellular Compartmentation and Differential Catalytic Properties of the Three Human Nicotinamide Mononucleotide Adenylyltransferase Isoforms." *J Biol Chem* 280, no. 43 (Oct 28): 36334-41. https://dx.doi.org/10.1074/jbc.M508660200.

Bradford, M. M. 1976. "A Rapid and Sensitive Method for the Quantitation of Microgram Quantities of Protein Utilizing the Principle of Protein-Dye Binding." *Anal Biochem* 72 (May 07): 248-54. https://dx.doi.org/10.1006/abio.1976.9999.

Brunelle, J. L., and R. Green. 2014. "One-Dimensional Sds-Polyacrylamide Gel Electrophoresis (1d Sds-Page)." *Methods Enzymol* 541: 151-9. https://dx.doi.org/10.1016/B978-0-12-420119-4.00012-4.

Chafik, A., A. Essamadi, S. Y. Çelik, and A. Mavi. 2020. "A Novel Acid Phosphatase from Cactus (Opuntia Megacantha Salm-Dyck) Cladodes: Purification and Biochemical Characterization of the Enzyme." *Int J Biol Macromol* 160 (Oct 01): 991-999. https://dx.doi.org/10.1016/j.ijbiomac.2020.05.175.

Chen, V. B., W. B. Arendall, J. J. Headd, D. A. Keedy, R. M. Immormino, G. J. Kapral, L. W. Murray, J. S. Richardson, and D. C. Richardson. 2010. "Molprobity: All-Atom Structure Validation for Macromolecular Crystallography." *Acta Crystallogr D Biol Crystallogr* 66, no. Pt 1 (Jan): 12-21. https://dx.doi.org/10.1107/S0907444909042073.

Chiang, P. W., J. Wang, Y. Chen, Q. Fu, J. Zhong, X. Yi, R. Wu, H. Gan, Y. Shi, C. Barnett, D. Wheaton, M. Day, J. Sutherland, E. Heon, R. G. Weleber, L. A. Gabriel, P. Cong, K. Chuang, S. Ye, J. M. Sallum, and M. Qi. 2012. "Exome Sequencing Identifies Nmnat1 Mutations as a Cause of Leber Congenital Amaurosis." *Nat Genet* 44, no. 9 (Sep): 972-4. https://dx.doi.org/10.1038/ng.2370.

Cianci, M., G. Bourenkov, G. Pompidor, I. Karpics, J. Kallio, I. Bento, M. Roessle, F. Cipriani, S. Fiedler, and T. R. Schneider. 2017. "P13, the Embl Macromolecular Crystallography Beamline at the Low-Emittance Petra Iii Ring For high- and Low-Energy Phasing with Variable Beam Focusing." *J Synchrotron Radiat* 24, no. Pt 1 (Jan 01): 323-332. https://dx.doi.org/10.1107/S1600577516016465.

Clamp, M., J. Cuff, S. M. Searle, and G. J. Barton. 2004. "The Jalview Java Alignment Editor." *Bioinformatics* 20, no. 3 (Feb 12): 426-7. https://dx.doi.org/10.1093/bioinformatics/btg430.

D'Angelo, I., N. Raffaelli, V. Dabusti, T. Lorenzi, G. Magni, and M. Rizzi. 2000. "Structure of Nicotinamide Mononucleotide Adenylyltransferase: A Key Enzyme in Nad(+) Biosynthesis." *Structure* 8, no. 9 (Sep 15): 993-1004. https://dx.doi.org/10.1016/s0969-2126(00)00190-8.

Di Martino, C., and M. L. Pallotta. 2011. "Mitochondria-Localized Nad Biosynthesis by Nicotinamide Mononucleotide Adenylyltransferase in Jerusalem Artichoke (Helianthus Tuberosus L.) Heterotrophic Tissues." *Planta* 234, no. 4 (Oct): 657-70. https://dx.doi.org/10.1007/s00425-011-1428-6.

Emanuelli, M., F. Carnevali, F. Saccucci, F. Pierella, A. Amici, N. Raffaelli, and G. Magni. 2001. "Molecular Cloning, Chromosomal Localization, Tissue Mrna Levels, Bacterial Expression, and Enzymatic Properties of Human Nmn Adenylyltransferase." *J Biol Chem* 276, no. 1 (Jan 05): 406-12. https://dx.doi.org/10.1074/jbc.M008700200.

Emsley, P., and K. Cowtan. 2004. "Coot: Model-Building Tools for Molecular Graphics." *Acta Crystallogr D Biol Crystallogr* 60, no. Pt 12 Pt 1 (Dec): 2126-32. https://dx.doi.org/10.1107/S0907444904019158.

Foster, J. W., E. A. Holley-Guthrie, and F. Warren. 1987. "Regulation of Nad Metabolism in Salmonella Typhimurium: Genetic Analysis and Cloning of the Nadr Repressor Locus." *Mol Gen Genet* 208, no. 1-2 (Jun): 279-87. https://dx.doi.org/10.1007/BF00330454.

Garavaglia, S., I. D'Angelo, M. Emanuelli, F. Carnevali, F. Pierella, G. Magni, and M. Rizzi. 2002. "Structure of Human Nmn Adenylyltransferase. A Key Nuclear Enzyme for Nad Homeostasis." *J Biol Chem* 277, no. 10 (Mar 08): 8524-30. https://dx.doi.org/10.1074/jbc.M111589200.

Gerdes, S, C Lerma-Ortiz, O Frelin, SMD Seaver, CS Henry, V de Crecy-Lagard, and AD Hanson. 2012. "Plant B Vitamin Pathways and Their Compartmentation: A Guide for the Perplexed." *Journal of Experimental Botany* 63, no. 15 (SEP 2012): 5379-5395. https://dx.doi.org/10.1093/jxb/ers208.

Gerdes, S. Y., O. V. Kurnasov, K. Shatalin, B. Polanuyer, R. Sloutsky, V. Vonstein, R. Overbeek, and A. L. Osterman. 2006. "Comparative Genomics of Nad Biosynthesis in Cyanobacteria." *J Bacteriol* 188, no. 8 (Apr): 3012-23. https://dx.doi.org/10.1128/JB.188.8.3012-3023.2006.

Gilley, J., and M. P. Coleman. 2010. "Endogenous Nmnat2 Is an Essential Survival Factor for Maintenance of Healthy Axons." *PLoS Biol* 8, no. 1 (Jan 26): e1000300. https://dx.doi.org/10.1371/journal.pbio.1000300.

Han, S., M. D. Forman, P. Loulakis, M. H. Rosner, Z. Xie, H. Wang, D. E. Danley, W. Yuan, J. Schafer, and Z. Xu. 2006. "Crystal Structure of Nicotinic Acid Mononucleotide Adenylyltransferase from Staphyloccocus Aureus: Structural Basis for Naad Interaction in Functional Dimer." *J Mol Biol* 360, no. 4 (Jul 21): 814-25. https://dx.doi.org/10.1016/j.jmb.2006.05.055.

Hashida, S. N., H. Takahashi, M. Kawai-Yamada, and H. Uchimiya. 2007. "Arabidopsis Thaliana Nicotinate/Nicotinamide Mononucleotide Adenyltransferase (Atnmnat) Is Required for Pollen Tube Growth." *Plant J* 49, no. 4 (Feb): 694-703. https://dx.doi.org/10.1111/j.1365-313X.2006.02989.x.

Hashida, S. N., T. Itami, H. Takahashi, K. Takahara, M. Nagano, M. Kawai-Yamada, K. Shoji, F. Goto, T. Yoshihara, and H. Uchimiya. 2010. "Nicotinate/Nicotinamide Mononucleotide Adenyltransferase-Mediated Regulation of Nad Biosynthesis Protects Guard Cells from Reactive Oxygen Species in Aba-Mediated Stomatal Movement in Arabidopsis." *J Exp Bot* 61, no. 13 (Aug): 3813-25. https://dx.doi.org/10.1093/jxb/erq190.

Hashida, S. N., H. Takahashi, and H. Uchimiya. 2009. "The Role of Nad Biosynthesis in Plant Development and Stress Responses." *Ann Bot* 103, no. 6 (Apr): 819-24. https://dx.doi.org/10.1093/aob/mcp019.

Holm, L. 2020. "Using Dali for Protein Structure Comparison." *Methods Mol Biol* 2112: 29-42. https://dx.doi.org/10.1007/978-1-0716-0270-6_3.

Hunt, L., F. Lerner, and M. Ziegler. 2004. "Nad - New Roles in Signalling and Gene Regulation in Plants." *New Phytol* 163, no. 1 (Jul): 31-44. https://dx.doi.org/10.1111/j.1469-8137.2004.01087.x.

Huppke, P., E. Wegener, J. Gilley, C. Angeletti, I. Kurth, J. P. H. Drenth, C. Stadelmann, A. Barrantes-Freer, W. Brück, H. Thiele, P. Nürnberg, J. Gärtner, G. Orsomando, and M. P. Coleman. 2019. "Homozygous Nmnat2 Mutation in Sisters with Polyneuropathy and Erythromelalgia." *Exp Neurol* 320 (10): 112958. https://dx.doi.org/10.1016/j.expneurol.2019.112958.

Jayaram, H. N., P. Kusumanchi, and J. A. Yalowitz. 2011. "Nmnat Expression and Its Relation to Nad Metabolism." *Curr Med Chem* 18, no. 13: 1962-72. https://dx.doi.org/10.2174/092986711795590138.

Joosten, R. P., F. Long, G. N. Murshudov, and A. Perrakis. 2014. "The Pdb_Redo Server for Macromolecular Structure Model Optimization." *IUCrJ* 1, no. Pt 4 (Jul 01): 213-20. https://dx.doi.org/10.1107/S2052252514009324.

Kabsch, W. 2010. "Xds." *Acta Crystallogr D Biol Crystallogr* 66, no. Pt 2 (Feb): 125-32. https://dx.doi.org/10.1107/S0907444909047337.

Kelley, L. A., S. Mezulis, C. M. Yates, M. N. Wass, and M. J. Sternberg. 2015. "The Phyre2 Web Portal for Protein Modeling, Prediction and Analysis." *Nat Protoc* 10, no. 6 (Jun): 845-58. https://dx.doi.org/10.1038/nprot.2015.053.

Krissinel, E., and K. Henrick. 2007. "Inference of Macromolecular Assemblies from Crystalline State." *J Mol Biol* 372, no. 3 (Sep 21): 774-97. https://dx.doi.org/10.1016/j.jmb.2007.05.022.

Kurnasov, O. V., B. M. Polanuyer, S. Ananta, R. Sloutsky, A. Tam, S. Y. Gerdes, and A. L. Osterman. 2002. "Ribosylnicotinamide Kinase Domain of Nadr Protein: Identification and Implications in Nad Biosynthesis." *J Bacteriol* 184, no. 24 (Dec): 6906-17. https://dx.doi.org/10.1128/JB.184.24.6906-6917.2002.

Laskowski, R. A., D. S. Moss, and J. M. Thornton. 1993. "Main-Chain Bond Lengths and Bond Angles in Protein Structures." *J Mol Biol* 231, no. 4 (Jun 20): 1049-67. https://dx.doi.org/10.1006/jmbi.1993.1351.

Lau, C., M. Niere, and M. Ziegler. 2009. "The Nmn/Namn Adenylyltransferase (Nmnat) Protein Family." *Front Biosci (Landmark Ed)* 14, no. 2 (01 01): 410-31. https://dx.doi.org/10.2741/3252.

Lau, C., C. Dölle, T. I. Gossmann, L. Agledal, M. Niere, and M. Ziegler. 2010. "Isoform-Specific Targeting and Interaction Domains in Human Nicotinamide Mononucleotide Adenylyltransferases." *J Biol Chem* 285, no. 24 (Jun 11): 18868-76. https://dx.doi.org/10.1074/jbc.M110.107631.

Liebschner, D., P. V. Afonine, N. W. Moriarty, B. K. Poon, O. V. Sobolev, T. C. Terwilliger, and P. D. Adams. 2017. "Polder Maps: Improving Omit Maps by Excluding Bulk Solvent." *Acta Crystallogr D Struct Biol* 73, no. Pt 2 (Feb 01): 148-157. https://dx.doi.org/10.1107/S2059798316018210.

Liu, F., A. Arias-Vásquez, K. Sleegers, Y. S. Aulchenko, M. Kayser, P. Sanchez-Juan, B. J. Feng, A. M. Bertoli-Avella, J. van Swieten, T. I. Axenovich, P. Heutink, C. van Broeckhoven, B. A. Oostra, and C. M. van Duijn. 2007. "A Genomewide Screen for Late-Onset Alzheimer Disease in a Genetically Isolated Dutch Population." *Am J Hum Genet* 81, no. 1 (Jul): 17-31. https://dx.doi.org/10.1086/518720.

Magni, G., A. Amici, M. Emanuelli, G. Orsomando, N. Raffaelli, and S. Ruggieri. 2004. "Structure and Function of Nicotinamide Mononucleotide Adenylyltransferase." *Curr Med Chem* 11, no. 7 (Apr): 873-85. https://dx.doi.org/10.2174/0929867043455666.

McCoy, A. J., R. W. Grosse-Kunstleve, P. D. Adams, M. D. Winn, L. C. Storoni, and R. J. Read. 2007. "Phaser Crystallographic Software." *J Appl Crystallogr* 40, no. Pt 4 (Aug 01): 658-674. https://dx.doi.org/10.1107/S0021889807021206.

Miwa, A., Y. Sawada, D. Tamaoki, M. Yokota Hirai, M. Kimura, K. Sato, and T. Nishiuchi. 2017. "Nicotinamide Mononucleotide and Related Metabolites Induce Disease Resistance against Fungal Phytopathogens in Arabidopsis and Barley." *Sci Rep* 7, no. 1 (07 25): 6389. https://dx.doi.org/10.1038/s41598-017-06048-8.

Murshudov, G. N., A. A. Vagin, and E. J. Dodson. 1997. "Refinement of Macromolecular Structures by the Maximum-Likelihood Method." *Acta Crystallogr D Biol Crystallogr* 53, no. Pt 3 (May 01): 240-55. https://dx.doi.org/10.1107/S0907444996012255.

Noctor, G, J Hager, SC Li, F Rebeille, and R Douce. 2011. "Biosynthesis of Nad and Its Manipulation in Plants." *Biosynthesis of Vitamins in Plants: Vitamins a, B1, B2, B3, B5, Pt a* 58 (2011): 153-201. https://dx.doi.org/10.1016/B978-0-12-386479-6.00002-0.

Olland, A. M., K. W. Underwood, R. M. Czerwinski, M. C. Lo, A. Aulabaugh, J. Bard, M. L. Stahl, W. S. Somers, F. X. Sullivan, and R. Chopra. 2002. "Identification, Characterization, and Crystal Structure of Bacillus Subtilis Nicotinic Acid Mononucleotide Adenylyltransferase." *J Biol Chem* 277, no. 5 (Feb 01): 3698-707. https://dx.doi.org/10.1074/jbc.M109670200.

Pérez-Bueno, M. L., J. Illescas-Miranda, A. F. Martín-Forero, A. de Marcos, M. Barón, C. Fenoll, and M. Mena. 2022. "An Extremely Low Stomatal Density Mutant Overcomes Cooling Limitations at Supra-Optimal Temperature by Adjusting Stomatal Size and Leaf Thickness." *Front Plant Sci* 13: 919299. https://dx.doi.org/10.3389/fpls.2022.919299.

Raffaelli, N., T. Lorenzi, A. Amici, M. Emanuelli, S. Ruggieri, and G. Magni. 1999a. "Synechocystis Sp. Slr0787 Protein Is a Novel Bifunctional Enzyme Endowed with Both Nicotinamide Mononucleotide Adenylyltransferase and 'Nudix' Hydrolase Activities." *FEBS Lett* 444, no. 2-3 (Feb 12): 222-6. https://dx.doi.org/10.1016/s0014-5793(99)00068-x.

Raffaelli, N., T. Lorenzi, P. L. Mariani, M. Emanuelli, A. Amici, S. Ruggieri, and G. Magni. 1999b. "The Escherichia Coli Nadr Regulator Is Endowed with Nicotinamide Mononucleotide Adenylyltransferase Activity." *J Bacteriol* 181, no. 17 (Sep): 5509-11. https://dx.doi.org/10.1128/JB.181.17.5509-5511.1999.

Raffaelli, N., L. Sorci, A. Amici, M. Emanuelli, F. Mazzola, and G. Magni. 2002. "Identification of a Novel Human Nicotinamide Mononucleotide Adenylyltransferase." *Biochem Biophys Res Commun* 297, no. 4 (Oct 04): 835-40. https://dx.doi.org/10.1016/s0006-291x(02)02285-4.

Rodionova, I. A., H. J. Zuccola, L. Sorci, A. E. Aleshin, M. D. Kazanov, C. T. Ma, E. Sergienko, E. J. Rubin, C. P. Locher, and A. L. Osterman. 2015. "Mycobacterial Nicotinate Mononucleotide

Adenylyltransferase: Structure, Mechanism, and Implications for Drug Discovery." *J Biol Chem* 290, no. 12 (Mar 20): 7693-706. https://dx.doi.org/10.1074/jbc.M114.628016.

Schweiger, M., K. Hennig, F. Lerner, M. Niere, M. Hirsch-Kauffmann, T. Specht, C. Weise, S. L. Oei, and M. Ziegler. 2001. "Characterization of Recombinant Human Nicotinamide Mononucleotide Adenylyl Transferase (Nmnat), a Nuclear Enzyme Essential for Nad Synthesis." *FEBS Lett* 492, no. 1-2 (Mar 09): 95-100. https://dx.doi.org/10.1016/s0014-5793(01)02180-9.

Segel, I.H. 1975. *Enzyme Kinetics*. pp. 274-275, Wiley, New York.

Sorci, L., F. Cimadamore, S. Scotti, R. Petrelli, L. Cappellacci, P. Franchetti, G. Orsomando, and G. Magni. 2007. "Initial-Rate Kinetics of Human Nmn-Adenylyltransferases: Substrate and Metal Ion Specificity, Inhibition by Products and Multisubstrate Analogues, and Isozyme Contributions to Nad+ Biosynthesis." *Biochemistry* 46, no. 16 (Apr 24): 4912-22. https://dx.doi.org/10.1021/bi6023379.

Sperschneider, J., A. M. Catanzariti, K. DeBoer, B. Petre, D. M. Gardiner, K. B. Singh, P. N. Dodds, and J. M. Taylor. 2017. "Localizer: Subcellular Localization Prediction of Both Plant and Effector Proteins in the Plant Cell." *Sci Rep* 7 (Mar 16): 44598. https://dx.doi.org/10.1038/srep44598.

Tagad, C. K., and S. G. Sabharwal. 2018. "Purification and Characterization of Acid Phosphatase From." *J Food Sci Technol* 55, no. 1 (Jan): 313-320. https://dx.doi.org/10.1007/s13197-017-2941-9.

Wang, S., J. Han, J. Xia, Y. Hu, L. Shi, A. Ren, J. Zhu, and M. Zhao. 2020. "Overexpression of Nicotinamide Mononucleotide Adenylyltransferase (Nmnat) Increases the Growth Rate, Ca." *Appl Microbiol Biotechnol* 104, no. 16 (Aug): 7079-7091. https://dx.doi.org/10.1007/s00253-020-10763-0.

Werner, E., M. Ziegler, F. Lerner, M. Schweiger, and U. Heinemann. 2002. "Crystal Structure of Human Nicotinamide Mononucleotide Adenylyltransferase in Complex with Nmn." *FEBS Lett* 516, no. 1-3 (Apr 10): 239-44. https://dx.doi.org/10.1016/s0014-5793(02)02556-5.

Willard, L., A. Ranjan, H. Zhang, H. Monzavi, R. F. Boyko, B. D. Sykes, and D. S. Wishart. 2003. "Vadar: A Web Server for Quantitative Evaluation of Protein Structure Quality." *Nucleic Acids Res* 31, no. 13 (Jul 01): 3316-9. https://dx.doi.org/10.1093/nar/gkg565.

Yalowitz, J. A., S. Xiao, M. P. Biju, A. C. Antony, O. W. Cummings, M. A. Deeg, and H. N. Jayaram. 2004. "Characterization of Human Brain Nicotinamide 5'-Mononucleotide Adenylyltransferase-2 and Expression in Human Pancreas." *Biochem J* 377, no. Pt 2 (Jan 15): 317-26. https://dx.doi.org/10.1042/BJ20030518.

Yoon, H. J., H. L. Kim, B. Mikami, and S. W. Suh. 2005. "Crystal Structure of Nicotinic Acid Mononucleotide Adenylyltransferase from Pseudomonas Aeruginosa in Its Apo and Substrate-Complexed Forms Reveals a Fully Open Conformation." *J Mol Biol* 351, no. 2 (Aug 12): 258-65. https://dx.doi.org/10.1016/j.jmb.2005.06.001.

Zaman, U., S. U. Khan, A. A. Hendi, K. U. Rehman, S. Badshah, M. S. Refat, A. M. Alsuhaibani, K. Ullah, and A. Wahab. 2022. "Kinetic and Thermodynamic Studies of Novel Acid Phosphatase Isolated and Purified from Carthamus Oxyacantha Seedlings." *Int J Biol Macromol* 224 (Dec 05): 20-31. https://dx.doi.org/10.1016/j.ijbiomac.2022.12.025.

Zaman, U., R. Naz, N. S. Khattak, K. U. Rehman, A. Saeed, M. Farooq, J. Sahar, and A. Iqbal. 2021. "Kinetic and Thermodynamic Studies of Novel Acid Phosphates Extracted from Cichorium Intybus Seedlings." *Int J Biol Macromol* 168 (Jan 31): 195-204. https://dx.doi.org/10.1016/j.ijbiomac.2020.12.032.

Zhang, H., T. Zhou, O. Kurnasov, S. Cheek, N. V. Grishin, and A. Osterman. 2002. "Crystal Structures of E. Coli Nicotinate Mononucleotide Adenylyltransferase and Its Complex with Deamido-Nad." *Structure* 10, no. 1 (Jan): 69-79. https://dx.doi.org/10.1016/s0969-2126(01)00693-1.

Zhang, X., O. V. Kurnasov, S. Karthikeyan, N. V. Grishin, A. L. Osterman, and H. Zhang. 2003. "Structural Characterization of a Human Cytosolic Nmn/Namn Adenylyltransferase and Implication in Human Nad Biosynthesis." *J Biol Chem* 278, no. 15 (Apr 11): 13503-11. https://dx.doi.org/10.1074/jbc.M300073200.

Zhou, T., O. Kurnasov, D. R. Tomchick, D. D. Binns, N. V. Grishin, V. E. Marquez, A. L. Osterman, and H. Zhang. 2002. "Structure of Human Nicotinamide/Nicotinic Acid Mononucleotide Adenylyltransferase. Basis for the Dual Substrate Specificity and Activation of the Oncolytic Agent Tiazofurin." *J Biol Chem* 277, no. 15 (Apr 12): 13148-54. https://dx.doi.org/10.1074/jbc.M111469200.

CHAPTER IV

PRODUCTION OF THE EXTRACELLULAR DOMAIN OF LECRK1.8 RECEPTOR

1. INTRODUCTION

Plants sensing of environmental and endogenous stimuli tends to be held at the functional continuum between Cell Wall- Plasma Membrane (CW-PM) and the interaction of specific ligands with the extracellular domains of transmembrane receptors situated on the CW determines morphological changes, adaptive and developmental responses.

Among over 600 receptor-like kinases present in *Arabidopsis*, literature distinguishes three groups based on the extracellular domain.

1. Wall-Associated Kinases (WAKs)
2. Proline-rich Extracellular Receptor Kinases (PERKs)
3. Lectin Receptor Kinases (LecRKs)

While the first two groups are related to structural changes (cell integrity, shape and turgor regulation), or physiological changes (hormonal responses and plant growth), the third group comprises receptors mostly involved in plant defence mechanisms and immunity (Nakhamchik et al. 2004; Shiu and Bleecker 2001; Kim et al. 2010; Anderson et al. 2001).

The polypeptide chain of a typical LecRK possesses a lectin-like ectodomain able to bind carbohydrates, a transmembrane hydrophobic domain, crucial for its localization in the plasma membrane and for the dimerization with other transmembrane proteins. (Bi et al. 2016), and a C-terminal intracellular domain, commonly characterized by a Ser/Thr kinase or a tyrosine kinase activity dependent on divalent cations. This domain specifically interacts with and phosphorylates downstream signalling molecules, such as the members of the mitogen-activated protein kinase (MAPK) cascade. (Singh et al. 2012). Based on their lectin-like motif, LecRKs are usually subdivided in three categories: G-, C- and L-type legume like LecRKs.

The L-type LecRKs have been studied since the early 2000. Transcriptome profile of the genes coding for these receptors considerably changes after treatment with both salicylic acid and other defence-related compounds and under several abiotic stresses. Similarly, the expression of many L-type LecRKs is strongly induced by bacterial LPS (Bouwmeester and Govers 2009).

Few years ago, a non-selective eNAD(P)$^+$ receptor, belonging to L-type LecRKs, was identified in LecRK-VI.2 (Singh, et al. 2012). This receptor complexes *in vivo* with Brassinosteroid insensitive-Associated Kinase 1 (BAK1), which is involved in multiple signalling pathways including brassinosteroid signalling, as well as in PAMP-triggered immunity, cell-death control and anther's development regulation (Yasuda, Okada, and Saijo 2017). Interestingly, both the kinase activities of LecRK-VI.2 and BAK1 are essential for eNAD(P)$^+$-mediated SAR signalling. It was proposed a

transphosphorylation between these receptors upon eNAD(P)$^+$ binding to LecRK-VI.2 pocket. Final acceptor in the intracellular phosphorylation cascade would be the nuclear transcription factor called NON-EXPRESSOR OF PATHOGEN-RELATED GENES1 (NPR1) (Wang, et al. 2019; Backer, Naidoo, and van den Berg 2019). NPR1 protein is the key regulator of SAR: in its unphosphorylated state it can be found as a large cytoplasmic oligomer. Phosphorylation determines the NPR1 monomerization and NPR1 monomers are subsequently activated upon direct binding to SA and consequently translocated to the nucleus where they stimulate PRGs expression (Cao et al. 1997).

LecRK1.8 was identified as the first specific eNAD$^+$ receptor able to sense NAD$^+$ resulting in the stimulation of PRGs expression. In fact, eNADP$^+$ does not compete with NAD$^+$ for binding. In 2017, a microarray analysis revealed that a group of receptor-like kinases, including LecRK1.8, were induced by exogenous application of NAD$^+$. Specific *Arabidopsis* mutants lacking the gene coding for LecRK1.8 were isolated for further transcriptome analysis. An additional mutant for *dorn-1* was used as control; this gene is implicated in plant systemic acquired resistance, but it does not respond to nucleotides. When exogenous NAD$^+$ was given to WT and *dorn-1* mutants PRG levels increased. On the other hand, mutants for the receptor showed only a weak increase, indicating the specific involvement of the receptor in NAD$^+$ induction of PRGs.

The binding of NAD$^+$ to the receptor was confirmed by overexpressing the extracellular domain of LecRK1.8 fused with GFP in transgenic plants, by its purification through immunoprecipitation and binding assay with radio-labelled NAD$^+$. The eLecRK1.8-GFP fusion protein showed a remarkable affinity for NAD$^+$, with a K_d value of 436.5 ± 104.8 nM (Wang, et al. 2017).

In this part of the thesis, in order to give an insight into NAD$^+$-dependent plant immunity, we aimed to produce the eLecRK1.8 extracellular domain in a recombinant form to study its binding to NAD$^+$ from a structural point of view. During my PhD research activity, the cDNA of eLecRK1.8 was cloned and the domain was expressed in insect cells.

2. EXPERIMENTAL PROCEDURES

2.1. Molecular Cloning of eLecRK 1.8

The coding sequence of the extracellular domain (aa 23-283, GenPept accession number: Q9LSR9) of eLecRK1.8 from *A. thaliana*, harboured in pMALp2X plasmid, was used as template for DNA amplification using CloneAmp® HiFi Taq Polymerase and the primers in Table 1. PCR cycles were set as follow: 30 cycles of denaturation (98°C for 10 sec), annealing (55°C for 10 sec) and extension (72°C for 5 sec).

Name	Sequence	Tm°C	CG%	nt	A	T	C	G	Extinction coefficient (1/(mM·cm))	Molecular weight (g/mol)
Fw	5'-gcctttgcggccatgcaacaagaaactggcttcagc-3'	76.9	56	36	9	7	11	9	334.5	11030
Rv	5'-tgctcgagtgcggccgcgagagaagttttcattttaggatga-3'	73.4	50	42	9	12	7	14	407.7	13040

Table 1. Primers for eLecRK1.8 cloning.

The amplified fragment was cloned into the pBAC3 vector by using the In-Fusion® HD recombinant technology. The vector was linearized with *Nco*I and *Not*I FastDigest™ restriction enzymes (Thermo Scientific).The complete linearization of pBAC3 and the amplification of the fragment were checked on 1% agarose gel. The recombinant mixture was transformed into STELLAR™ chemically competent cells and positivity of clones was checked through enzymatic digestion of the extracted plasmids. Sanger sequencing confirmed the lack of mutations in the recombinant plasmid pBAC3-eLecRK1.8 used for the expression of the receptor.

2.2. Insect cells transfection and virus amplification

The recombinant baculovirus containing the gene of interest was obtained by using the BacMagic™ Transfection kit (Novagen). Homologous recombination between pBAC3-eLecRK1.8 construct and the empty viral genome occurred in SF9 insect cells growing in adhesion in 35-mm plates at 28°C. A transfection mixture was prepared according to manufacturer's instructions. The transfection was performed by adding 1 ml of transfection mixture to cells monolayers ensuring a multiplicity of infection (MOI) of 0.017. After overnight incubation at 28°C in a flat-bottomed covered storage container, viral population was harvested and stored in dark at 4°C until use. The obtained viral population was subjected to a series of amplifications to increase the viral titer. In each amplification step the titer was quantified through plaque assay (see paragraph 2.3.). Amplification steps were carried out in SF9 cells cultures (20 ml), exponentially growing in suspension. When the titer reached the value of at least $5x10^7$ pfu/ml, the viral population was used for the expression.

2.3. Plaque Assay

Viral stocks titer was determined by infecting 1 million of SF9 cells growing in adhesion in 35-mm plates. Infection was performed with ten-fold serial dilutions of the viral population, starting from a 10^{-1} dilution in which 100 µl of undiluted viral population were added to room temperature BacVector® Insect Cell Medium up to a final volume of 1 ml. The number of dilutions was depending on the viral titer expected. After 1 hour incubation at room temperature, virus inoculum was removed and a solution of 1/3 of 3% BacPlaque™ Agarose and 2/3 of Express Five™ Serum Free Medium was added to each layer of cells. Plates were incubated at room temperature until the agarose-medium

was completely solidified. Finally, each well surface was covered with additional growth medium and incubated for 3-4 days at 28°C in a flat-bottomed covered humid container. Plaque staining was performed by substituting the growth medium layer with 0.33% (w/v) of Neutral Red stain, diluted 1:13 in PBS buffer. After 2 hours incubation at 28°C, staining solution was removed and plaques were identified and counted.

2.4. Expression of eLecRK 1.8

Protein expression was induced by transfection of an exponentially growing culture (20 ml) of High Five™ insect cells. Expression trials were conducted varying MOI from 2 to 8 in cultures of about 2 $x10^6$ cells/ml. Proteolysis of the receptor was avoided by directly adding to the culture medium the Sigma® Protease Inhibitor cocktail designed for use in tissue culture media diluted 1:800 and Fetal Bovine Serum (FBS) up to a final concentration of 0.5% (v/v). Cells were collected at different times fromthe infection, centrifuged for 10 minutes at 10.000 g, at 4°C, and discarded. Supernatants were subjected to a second centrifugation for virions removal (1 hour at 16.000 g, at 4°C). The presence ofthe receptor in the medium was evaluated by Western blot analysis. The protein content was determined by the Bradford method (Bradford 1976).

2.5. Western blot analysis

Samples of growth medium after 0, 24, 48 and 72 hours from infection were loaded in a 15% polyacrylamide gel and were subjected to SDS-PAGE (Brunelle and Green 2014). Bands were blotted onto a nitrocellulose membrane using the Trans-Blot® Turbo™ Transfer System (BioRad). Membrane was washed with TBS buffer (20 mM Tris HCl pH 7.6, 137 mM NaCl) for 5 min and incubated for 1 hour in a solution of 5% (w/v) dried milk resuspended in TTBS buffer (20 mM Tris HCl pH 7.6, 137 mM NaCl, 0.1%(v/v) Tween 20). The primary antibody (goat anti-6x His, Takara®) was diluted 1:5,000 in the same solution and incubated overnight with the membrane at 4°C. The following day, membrane was firstly washed three times in TTBS, then incubated with secondary antibody (mouse anti-goat, HRP-conjugated, Bio-Rad®) diluted 1:3000, and bands revelation occurred by adding 1:1 Luminol and horseradish peroxidase from the Clarity™ Western ECL kit (Bio-Rad®). Bands luminescence was detected in Chemidoc XRS^+ Imaging System Bio-Rad®.

3. RESULTS

Production of the extracellular domain of LecRK 1.8

In order to shed light onto the NAD^+-mediated plant immunity systems and on the role of extracellular NAD^+ as signalling molecule, we aimed to produce and functionally characterize the extracellular domain of LecRK1.8 (eLecRK1.8). The cDNA sequence of the full receptor (ID: BAD93956.1 in the European Nucleotide Archive, ENA) is shown in Figure 1. Nucleotides 67-849 correspond to the extracellular domain which has been described to be able to selectively bind NAD^+ (Wang, et al. 2017). This sequence had been previously cloned into pMAL2pX vector, for the expression in *E. coli* of the domain fused with the Maltose Binding Protein (MBP) (Wang, et al. 2017). In our lab the recombinant fused protein was expressed, however the receptor domain resulted to be insoluble after cleavage of the MBP, precluding its use for functional studies.

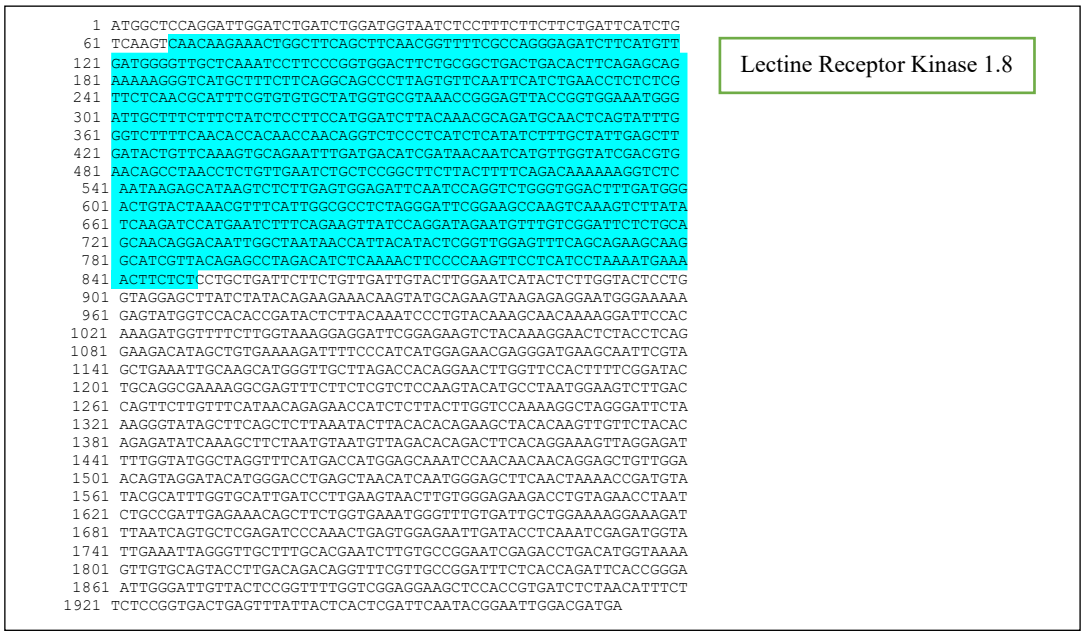

Figure 1. BAD93956.1 cDNA encoding for full-length LecRK1.8. Extracellular domain is highlighted in cyan.

For this reason, the eLecRK1.8 was subcloned into the pBAC3 vector, suitable for the baculovirus-mediated expression in insect cells. Subcloning and protein expression are described in Experimental Procedures. In order to establish the best expression conditions, several experiments were carried out by testing different MOI and growth media, using cultures growing both in adhesion and in suspension. In all tested conditions, a band of the expected molecular weight of eLecRK1.8 was detected through Western Blot analysis of the culture medium after incubation with anti-6His-tag antibody. Figure 2 shows the results obtained by infecting a suspension culture of High Five™ cells (1.3×10^6 cells/ml) at MOI 2. The expression of the protein was evident at 24 hours from infection,

but the band intensity decreased at 48 h and fully disappeared at72 h, suggesting that proteases in the medium might cleave eLecRK1.8 after its secretion.

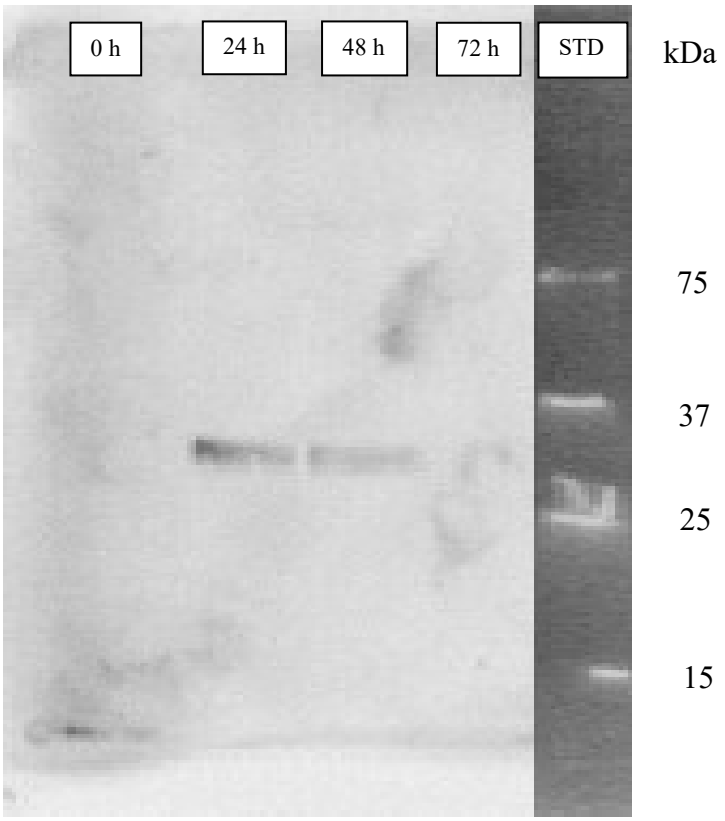

Figure 2. Western blot analysis of eLecRK1.8 expression level in the medium after 0, 24, 48 and 72 hours from the insect cells infection.

We therefore performed a screening in 24-well plates, testing different MOI (2, 4, 6 and 8) and adding a cocktail of proteases' inhibitors at 24 hours from infection in the culture medium of cells grown both in absence and in presence of 0.5% FBS (v/v). In the absence of FBS, the best expression was obtained at 24 h from the infection, but the protein levels decreased at 48h and totally disappeared at 72 h. In wells containing FBS, the expression peak occurred at 48 hours from infection and the band was still present at 72 hours. The same results were obtained at all tested MOI values.

In a subsequent experiment, the effect of growth medium renewal on the expression levels was tested in the presence of proteases' inhibitors added at 24 hours from infection. The medium renewal was performed just before the infection. A parallel culture with the same cell density (1.8 x10^6 cells/ml) was maintained in the spent medium. In both media we detected a band of comparable intensity at 24 hours, which fully disappeared at 48 h in the fresh medium, but not in the spent medium (Figure 3).

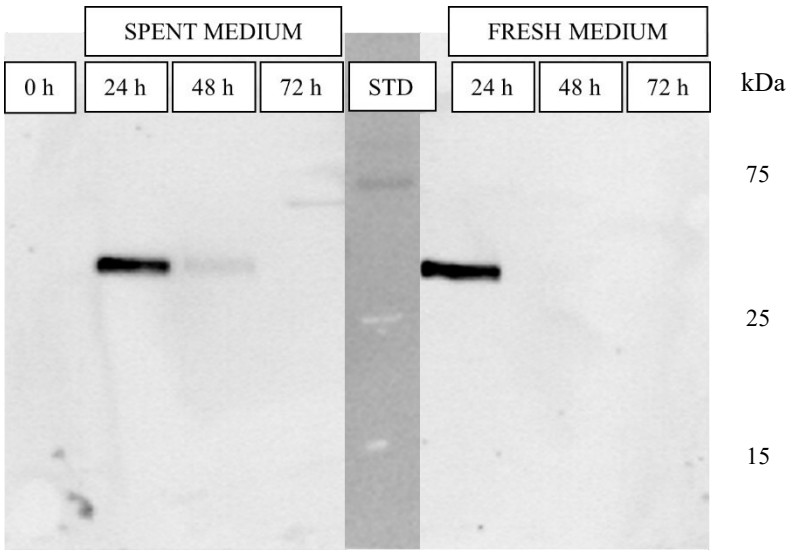

Figure 3. Western Blot Analysis of eLecRK1.8 expression level in fresh and spent growth medium at different times after infection.

Based on the above results, we scaled-up the expression by infecting exponentially growing cells at MOI 2. Before infection, growth medium was not renewed, but it was supplied with 0.5% FBS (v/v) and proteases' inhibitors were added at24 h from infection. The results are shown in Figure 4. The highest expression level was obtained at 48 h from the infection. We estimated a yield of less than 5 µg of protein starting from 150 ml culture, which is too low for further functional studies.

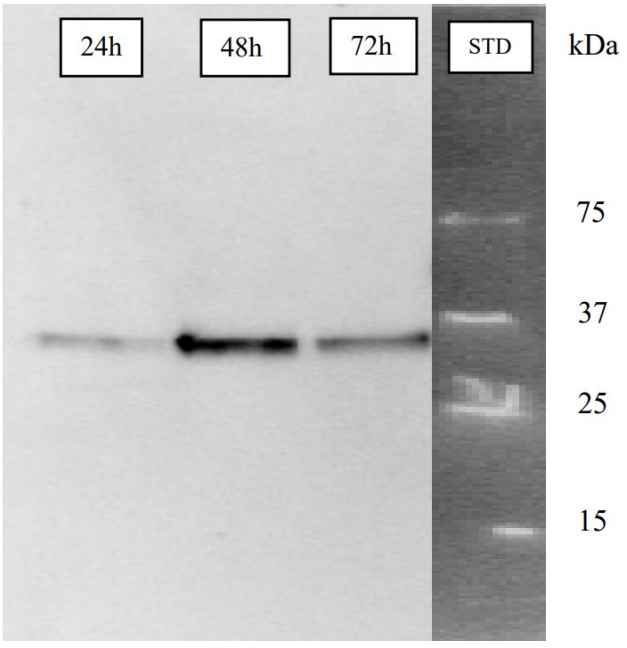

Figure 4. Western blot analysis of eLecRK1.8 expression level in the cell medium after 24, 48, 72 hours from the infection under optimized conditions

References

Anderson, C. M., T. A. Wagner, M. Perret, Z. H. He, D. He, and B. D. Kohorn. 2001. "Waks: Cell Wall-Associated Kinases Linking the Cytoplasm to the Extracellular Matrix." *Plant Mol Biol* 47, no. 1-2 (Sep): 197-206. https://dx.doi.org/10.1007/978-94-010-0668-2_12

Backer, R., S. Naidoo, and N. van den Berg. 2019. "The Nonexpressor of Pathogenesis-Related Genes 1 (Npr1) and Related Family: Mechanistic Insights in Plant Disease Resistance." *Front Plant Sci* 10: 102. https://dx.doi.org/10.3389/fpls.2019.00102.

Bi, G., T. W. Liebrand, R. R. Bye, J. Postma, A. M. van der Burgh, S. Robatzek, X. Xu, and M. H. Joosten. 2016. "Sobir1 Requires the Gxxxg Dimerization Motif in Its Transmembrane Domain to Form Constitutive Complexes with Receptor-Like Proteins." *Mol Plant Pathol* 17, no. 1 (Jan): 96-107. https://dx.doi.org/10.1111/mpp.12266.

Bouwmeester, K., and F. Govers. 2009. "Arabidopsis L-Type Lectin Receptor Kinases: Phylogeny, Classification, and Expression Profiles." *J Exp Bot* 60, no. 15: 4383-96. https://dx.doi.org/10.1093/jxb/erp277.

Bradford, M. M. 1976. "A Rapid and Sensitive Method for the Quantitation of Microgram Quantities of Protein Utilizing the Principle of Protein-Dye Binding." *Anal Biochem* 72 (May 07): 248-54. https://dx.doi.org/10.1006/abio.1976.9999.

Cao, H., J. Glazebrook, J. D. Clarke, S. Volko, and X. Dong. 1997. "The Arabidopsis Npr1 Gene That Controls Systemic Acquired Resistance Encodes a Novel Protein Containing Ankyrin Repeats." *Cell* 88, no. 1 (Jan 10): 57-63. https://dx.doi.org/10.1016/s0092-8674(00)81858-9.

Kim, Y. T., J. Oh, K. H. Kim, J. Y. Uhm, and B. M. Lee. 2010. "Isolation and Characterization of Ngrlk1, a Receptor-Like Kinase of Nicotiana Glutinosa That Interacts with the Elicitin of Phytophthora Capsici." *Mol Biol Rep* 37, no. 2 (Feb): 717-27. https://dx.doi.org/10.1007/s11033-009-9570-y.

Nakhamchik, A., Z. Zhao, N. J. Provart, S. H. Shiu, S. K. Keatley, R. K. Cameron, and D. R. Goring. 2004. "A Comprehensive Expression Analysis of the Arabidopsis Proline-Rich Extensin-Like Receptor Kinase Gene Family Using Bioinformatic and Experimental Approaches." *Plant Cell Physiol* 45, no. 12 (Dec): 1875-81. https://dx.doi.org/10.1093/pcp/pch206.

Shiu, S. H., and A. B. Bleecker. 2001. "Plant Receptor-Like Kinase Gene Family: Diversity, Function, and Signaling." *Sci STKE* 2001, no. 113 (Dec 18): re22. https://dx.doi.org/10.1126/stke.2001.113.re22.

Singh, P., Y. C. Kuo, S. Mishra, C. H. Tsai, C. C. Chien, C. W. Chen, M. Desclos-Theveniau, P. W. Chu, B. Schulze, D. Chinchilla, T. Boller, and L. Zimmerli. 2012. "The Lectin Receptor

Kinase-Vi.2 Is Required for Priming and Positively Regulates Arabidopsis Pattern-Triggered Immunity." *Plant Cell* 24, no. 3 (Mar): 1256-70. https://dx.doi.org/10.1105/tpc.112.095778.

Wang, C., X. Huang, Q. Li, Y. Zhang, J. L. Li, and Z. Mou. 2019. "Extracellular Pyridine Nucleotides Trigger Plant Systemic Immunity through a Lectin Receptor Kinase/Bak1 Complex." *Nat Commun* 10, no. 1 (10 22): 4810. https://dx.doi.org/10.1038/s41467-019-12781-7.

Wang, C., M. Zhou, X. Zhang, J. Yao, Y. Zhang, and Z. Mou. 2017. "A Lectin Receptor Kinase as a Potential Sensor for Extracellular Nicotinamide Adenine Dinucleotide In." *Elife* 6 (07 19). https://dx.doi.org/10.7554/eLife.25474.

Yasuda, S., K. Okada, and Y. Saijo. 2017. "A Look at Plant Immunity through the Window of the Multitasking Coreceptor Bak1." *Curr Opin Plant Biol* 38 (Aug): 10-18. https://dx.doi.org/10.1016/j.pbi.2017.04.007.

CHAPTER V

CONCLUSIONS

The metabolism of the various forms of vitamin B3 in plants affects not only key biochemical pathways, like photosynthesis and respiration, but also impacts on important developmental processes, such as seed germination, reproduction, and immunity. The enzyme NaMN/NMN adenylyltransferase, which catalyses an essential reaction, common to all metabolic routes generating NAD^+ from the various forms of vitamin B3, is essential for pollen tubes growth, seeds germination, resistance against phytopathogens and the recovery of stomatal guard cells under oxidative stress. The enzyme has been very poorly characterized, and here we report a comprehensive biochemical and structural characterization of the protein from *A. thaliana* (AraAT). We found that the plant enzyme closely resembles the bacterial counterpart, showing a strict specificity for the deamidated form of the pyridine mononucleotide substrate. This indicates that in plant, differently from mammals and similarly to most bacterial species, NAD^+ is preferentially synthetized through deamidated routes which generate the pyridine mononucleotide moiety of the coenzyme from nicotinic acid or from nicotinamide after its deamidation to nicotinic acid. The prevalence of the deamidated pathways in plant might be due to the higher chemical stability of the deamidated intermediates compared with the amidated ones, which might ensure the occurrence of the pathway also at high temperatures. In keeping with this, we also found that the AraAT is a rather thermophilic enzyme, with an optimal temperature at 50°C. By solving the three-dimensional structure of the plant enzyme in its apo-form and in complex with amidated and deamidated substrates and products, we have identified the molecular determinants responsible of the substrate specificity. Besides, we can now rely on structures of representative enzymes from all three kingdoms of life.

In last decades, the importance of NAD^+ was expanded to its function outside the plant cells, where it acts as a signalling molecule. When released from damaged or dying cells, extracellular NAD^+ ($eNAD^+$) acts as a Damage Associated Molecular pattern (DAMP), which is sensed by cell surface receptors and triggers an immune response against pathogens. Recently, LecRK1.8 was identified as a highly specific $eNAD^+$ receptor, able to bind $eNAD^+$ and to trigger immunity-related signals resulting in resistance responses. However, the molecular mechanism linking $eNAD^+$ to immunity is still matter of investigation. Our aim was to produce in a recombinant form the extracellular domain of the receptor to confirm its ability to bind NAD^+. To this end, we expressed the protein in insect cells using the baculovirus system. However, despite several attempts, we were not able to produce the receptor in suitable amount for further functional studies.